



Capstone Thesis

Hybrid Rocket Engine Optimization through Open Loop Control

Author: Aleksandr Hakobyan

Supervisor: Hrachya Kocharyan

Institution: American University of Armenia

15.05.2023

Acknowledgement

To begin with I would like to express my sincerest gratitude to my supervisor Dr. Hrachya Kocharyan for his support and guidance throughout the research process connected to this capstone thesis. Dr. Kocharyan encouraged me to pursue this research, even when it seemed like it was too complex, and never let me lose my spirit both as an individual and an academic. Thank you for believing in me and pushing me beyond what I thought I was capable of and for helping me see that the stars are truly the limit when it comes to something one is passionate about. I would also like to thank you for teaching me courses such as Material Science and especially Thermodynamics and Control Systems which were instrumental in shaping how I approach and solve big problems in the academic field and are now among the most useful tools in my Engineering portfolio.

I would like to continue by thanking the professors throughout my journey to becoming an Engineer at the American University of Armenia. I would like to thank Dr. Bilor Kurghinyan for challenging me with extracurricular projects related to electronics and circuitry. This helped me master the art of circuit design and finding solutions with limited components. I would also like to thank Vardan Hayrapetyan for fuelling my curiosity toward natural phenomena and chemical processes. Additionally, I would like to show my deepest appreciation to Mr. Arman Asatryan, facilities engineer of the Engineering Laboratory, for always being there to answer technical questions as well as support my projects which involved anything related to 3D printing and manufacturing.

I wish to extend a tremendous thank you to my peers and colleagues, especially Elizabeth Vickery, Hayk Tamazyan, Gor Isoyan, Aram Hovhannisyan, Krist Samuel Siraki, and Arman Babayan and alumni Grigor Tikharyan and Amaras Mehrabi for aiding me in peer-reviewing papers, solving issues in my projects, and overall being a backbone on which I have leaned on for many occasions. It is through their friendly spirit and support that I am where I am today.

To conclude, I would like to thank my parents Anna Kocharyan and Aram Hakobyan for believing in me throughout the entire process. I want to thank them for helping me overcome burnouts after so many late nights in the lab, and for teaching me that consistency is key to achieving success. I would not have been where I am without all that you have given me.

Abstract

Rocket engines are an essential component of delivering any payload such as satellites, rovers, and probes into space. One such kind of engine is the Hybrid Rocket Engine. Classical Hybrid Rocket Engines have first become popular in the early 1970s. These engines, while providing combined advantages of both Solid Rocket Motors and Liquid Rocket Engines, as well as being relatively cheap to manufacture when compared to Liquid Rocket Engines, exhibit drawbacks in thrust throughout the burn of the engine caused by the propellant ratio shifts induced by fuel regression. Their loss in efficiency is what makes them undesirable in the construction of rockets and causes companies to use the more expensive Liquid Rocket Engines which are higher in efficiency and overall thrust output. The negative side effects of this the fuel regression can be reduced by eliminating the propellant ratio shifts during the operation of a Hybrid Rocket Engine. This paper considers the use of open loop control techniques to nullify the regression effects and observe the effect this elimination has on the thrust output of the HYDRA 3X student-built Hybrid Rocket Engine as well as its change in efficiency for multiple different fuels. The differential equations of the fuel mass flowrate function are numerically solved in terms of oxidizer mass flowrate, the results of which are taken as a basis and three different fittings are suggested to define the control function. Based on the most optimal oxidizer control function two controllers are proposed in this paper. It was concluded that the Prometheus Open Loop Controller eliminates the propellant ratio shifts for all fuel types while decreasing overall thrust with larger flux exponent fuels, and the Epimetheus Open Loop Controller increases overall thrust and efficiency of the engine increasing with larger flux exponent fuels, but worsens the propellant ratio shifts during engine operation.

Glossary of Abbreviations

AP – Ammonium Perchlorate

APCP – Ammonium Perchlorate Composite Propellant

BCF – Belehradek Control Function

CECF – Composite Exponential Control Function

EOLC – Epimetheus Open Loop Controller

HRE – Hybrid Rocket Engine

HTPB – Hydroxyl Terminated Polybutadiene

IBCF – Inverse Belehradek Control Function

LOX – Liquid Oxygen

LH₂ – Liquid Hydrogen

LRE – Liquid Rocket Engine

PBAN – Polybutadiene Acrylonitrile

PCF – Power Control Function

POLC – Prometheus Open Loop Controller

SRM – Solid Rocket Motor

VAF – Valve Approximation Function

Table of Contents

Acknowledgement	2
Abstract.....	3
Glossary of Abbreviations	4
1.0 Literature review	7
1.1 General Introduction	7
1.2 Solid Rocket Motors	8
1.2.1 SRM History and Applications.....	8
1.2.2 Structure.....	9
1.2.3 Advantages and Disadvantages.....	10
1.3 Liquid Rocket Engines.....	11
1.3.1 LRE History and Applications.....	11
1.3.1 Structure.....	13
1.3.3 Advantages and Disadvantages.....	16
1.4 Hybrid Rocket Engines	17
1.4.1 HRE History and Applications	17
1.4.2 Structure.....	18
1.4.3 Advantages and Disadvantages.....	20
1.5 Aim of the Study.....	22
2.0 Theory and Mathematical Preliminaries	23
2.1 General Equations	23
2.2 Engine and Fuel Parameters.....	26
3.0 Results and Discussion	29
3.1 Mathematical Framework	29
3.2 Mathematical Approximations.....	31
3.2.1 Exponential Fitting (<i>MATLAB Curve Fitter</i>).....	31
3.2.2 Power Fitting (<i>MATLAB Curve Fitter</i>).....	34

3.2.3 Belehraddek Power Fitting (<i>Origin Pro</i>)	38
3.2.4 Engine Ignition Modelling	42
3.2.5 Prometheus Open Loop Controller	43
3.2.6 Epimetheus Open Loop Controller	45
3.3 Force Calculations	47
3.3.1 Calculations without a Controller	47
3.3.2 Calculations with POLC	49
3.3.3 Calculations with EOLC	50
4.0 Conclusions and Future Work	51
4.1 Conclusions.....	51
4.1.1 POLC	51
4.1.2 EOLC	53
4.1.3 Final Conclusions.....	56
4.2 Future Work.....	57
References.....	58

1.0 Literature review

1.1 General Introduction

Transportation has interested humankind throughout the history and many devices have been utilized by people to move heavy objects around faster and more efficiently. In the modern day these modes of transportation are boats – to be used on the water; bicycles, motorcycles, and cars – to be used on land; and rockets and planes – to be used in the air. These devices each play their role in aiding humanity in its development and perform tasks that people cannot on their own. Rockets solve several problems with regards to our current infrastructure on the planet. From launching new satellites into Earth orbit to support our communication from continent to continent, to sending people to space for extended periods of time in order to facilitate cutting the development of various scientific fields. The climate crisis our planet faces today would not be possible to monitor without the cutting-edge instrumentation orbiting earth providing updates on the status of forests and oceans [1]. This entire infrastructure has been created using powerful rockets which still help launch new satellites into orbit, transport crew to the International Space Station (ISS), and soon help humans reach the Moon again with the Artemis Mission [2]. Consequently, development of new rockets which are more reliable, powerful, and efficient will help all the causes mentioned even further.

One of the key components to a rocket is its engine. The engine is what propels the rocket forward and helps it counteract the force of gravity in order to send some payload into orbit or perhaps in a ballistic trajectory. Like all engines, rocket engines too come in various sizes and designs, however, the main purpose is always the same – produce thrust through a chemical reaction which in turn through Newtons Third Law of Motion will propel the rocket in the opposite direction with the same force. This is at heart the working principle of any rocket engine, although there are various types of engines.

There are three main categories of Rocket Engines based on their design and the type of fuel they use during their operation. These categories are Solid Rocket Motors (SRMs), Liquid Rocket Engines (LREs), and Hybrid Rocket Engines (HREs). Each has their own advantages and disadvantages and can be more suitable for one task than the other.

1.2 Solid Rocket Motors

1.2.1 SRM History and Applications

Solid Rocket Motors (SRMs) are rocket motors which use solid phase fuel and oxidizer proportionally mixed in the combustion chamber. The word motor is used when the propellant mixture is in a solid phase, in all other cases the device would be referred to as an engine [3]. SRMs are widely used in amateur rocketry and model rocket testing. One of the most important and large-scale uses of SRMs are as part of heavy launch vehicles in the form of Solid Rocket Boosters (SRBs) to provide the required thrust to launch particularly heavy payloads into space. Such SRBs can be seen attached radially to the main rocket body on launch vehicles like the Titan 3E (see *Figure 1a*), Space Shuttle Columbia launch vehicle (see *Figure 1b*), some Saturn family variants like the Saturn MLV 5-4SB, etc. [4]. SRMs are an essential part of artillery projectiles as well as emergency pilot escape mechanisms and upper stages of ballistic missiles [3].



*Figure 1a: Titan IIIE with
Voyager 2, August 20, 1977*
(© NASA)



*Figure 1b: Space Shuttle
Columbia, December 9, 2002*
(© NASA)

The aerospace field has seen different major developments and applications for SRMs. During the Second World War developments regarding tactical missiles which utilized solid propellants [4]. These developments in the military field further drove the research in castable

solid fuel grains. The tactical missile researched continued in the Atlantic Research Corporation, where Charles Henderson and Keith Rumbel found the addition of high amounts of Aluminium increased the Specific Impulse (I_{sp}) of the casted SRM [4]. The latter finding proved that this increase was tangential to HREs. This will be further covered in Sections 1.4.1 and 1.4.2 in greater detail.

SRMs are diverse in terms of choice of propellant. Solid Fuels and Oxidizers used range from sucrose ($C_6H_{12}O_6$) and potassium based garden fertilizer (KNO_3), used by beginner amateur rocket hobbyist nowadays, to polybutadiene acrylonitrile (PBAN) and ammonium perchlorate (AP or NH_3ClO_4) used in high end SRBs by NASA and other Space Agencies [5]. Solid Propellants and SRMs in general are known for their high thrust and low cost. One of the Ammonium perchlorate composite propellants (APCP) subcategory which is PBAN/AP listed above can have stage I_{sp} comparable to that of RP-1/LOX [6], which is a famous fuel and oxidizer combination for LREs (to be covered in Section 1.3 Liquid Rocket Engines), however, the overall I_{sp} of SRMs is relatively low when compared to overall I_{sp} of LREs.

1.2.2 Structure

SRMs are simple in their construction, consisting primarily of a Combustion Chamber, Propellant Grain, Ignitor Element, and a Nozzle. Due to the propellant being premixed with the correct static ratios of Oxidizer to Fuel (hereafter OF) there is no possible way to control the rate of combustion, consequently no way of regulating the thrust output of the motor. This decreases construction price of the motor, but the sacrifice of not regulating the OF ratio lowers the efficiency of the SRM significantly (to be discussed later in the section). In *Figure 2* you can an example of an SRM cross section can be observed with detailed description of the components [3] (note that some additional components like layer insulation and aft skirt can also be seen but are not essential to understanding the inner workings of an SRM).

An integral part of the motor is the fuel and oxidizer and the way they are cast. The propellant grain is geometrically a cylinder with an internal cavity where the combustion takes place (as can be seen in *Figure 2*). The internal cavity is referred to as the Grain Geometry and is one of the key components during SRM design as the surface area and burn regression determine the thrust profile of the engine and completeness of the burn. In order to achieve large amounts of thrust and high efficiency of combustion, industrially all the engines discussed in this paper

including SRMs are designed to accelerate the by-products of the internal chemical reaction past the speed of sound (Mach 1). For this purpose, the nozzles are designed having in mind that at the smallest cross-sectional area within the nozzle (also known as the *throat*) the velocity of the exhaust gasses should be Mach 1 for the diverging section to be able to further accelerate the gasses, achieving supersonic.

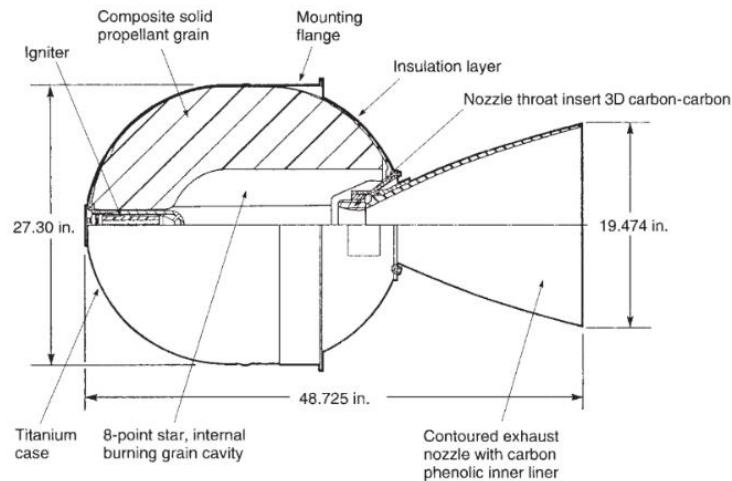


Figure 2: Solid Rocket Motor Cross Section, Source [3]

1.2.3 Advantages and Disadvantages

While there are applications for SRMs generally, even in those use cases solid propellant-based motors have distinct advantages and disadvantages. These are metrics come from design complexity, propellant phase, and type (premixed or injected oxidizer/fuel) and cost of construction and operation. The following section will underscore both in no necessary order of importance or impact.

Advantages

- High thrust – solid propellants have a high mass flow rate during launch for their size [7].
- Simplicity – these motors rarely if at all have moving parts and because of that are easier to construct when compared to HREs or LREs.
- Cost – because of the simplicity in construction and the fact that the propellant is premixed and in a solid state, there is no for expensive oxidizer or fuel

injection and pressurization systems, making SRMs the least expensive type of rocket motor.

- Storage stability – because of premixed fuel and oxidizer they can last upward of 30 years and still be utilized [7].

Disadvantages

- Not throttleable – once combustion is achieved it is very hard to stop as oxidizer is premixed with the fuel, therefore oxidizer to fuel ratio (hereafter OF) cannot be changed to vary thrust.
- Low I_{sp} – as covered in the section above, the overall I_{sp} for SRMs is much lower than that of LREs or HREs.

1.3 Liquid Rocket Engines

1.3.1 LRE History and Applications

Liquid Rocket Engines (LREs) are a type of rocket engine which operates on fuel and oxidizer in the liquid phase. Compared to SRMs they are complex in their construction and operation. LREs are the most widely used form of rocket propulsion due to their high I_{sp} , ability to be throttled, wide use of fuels and oxidizers, and substantially efficient combustion of the propellants. LREs are employed on rocket vehicles to launch humans and satellites into orbit, and on several high-speed research aircraft after WWII. Just like any rocket engine the gases produced after combustion are further accelerated through the use of a nozzle. This is what allows these engines to produce massive amounts of thrust propelling tons of payload along with the rocket body into space. Another difference from SRMs is the fact that the oxidizer is stored inside the rocket, allowing LREs to perform in the vacuum of space where there is no atmosphere. These engines are reliable, complex, and expensive to manufacture, however, their efficiency and thrust output is what makes them widely used until today.

Liquid rockets can be monopropellant (only one type of propellant) or bipropellant (two types of propellant). Tri-propellant rockets that use three different types of propellant are uncommon. Some designs can be throttled for variable thrust operation, and others can be restarted after an in-space shutdown. Liquid propellants are also used in hybrid rockets, which provide some of

the benefits of solid rockets. One of the most renowned LREs produced by in the United States is the main engine of the Space Shuttles produced by Rocketdyne by the name of Rocketdyne Aerojet, commonly known as RS-25. The RS-25 engine was used through 1981 to 2011 in all the Space Shuttle missions and is considered one of the greatest engines built burning for 8.5 minutes during the ascent of the space shuttle [8]. This engine is very versatile and will be used on the Space Launch System (SLS) rocket. See Figure 3 and Figure 4 below for visual aid.

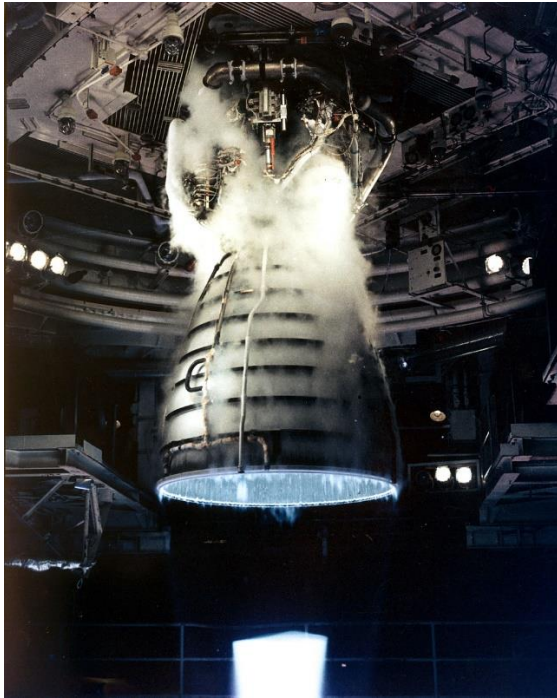


*Figure 3: RS-25 Liquid Rocket Engine, 1
January 1981, or 21 May 1981, (© NASA)*



*Figure 4: Space Launch System, 21
November 2022 (© NASA)*

Another considerable example of a relatively modern rocket engine is the Raptor-2 which is designed and manufactured by SpaceX. Raptor-2 is a revolutionary engine which uses Liquid Oxygen (LOX) and Liquid Methane (CH₄) as its fuel and oxidizer. Said engine has surpassed the famous Russian RD-180 and the previous generation RD-170 engines in their internal pressure and thrust output [9]. This is one of the greatest achievements made by the US Aerospace Industry as they no longer need to rely on the Russian Engines to power their rockets. The new engine has the capability to reach a chamber pressure of 26.89 MPa which is greater than the 26.7 MPa of the RD-180 [9]. See Figure 5 and Figure 6 below for visual reference on the engines mentioned.



Figure 5: Raptor-2 Liquid Rocket Engine, 22 May 2022, © Brandon/@bd_zero_g



Figure 6: RD-180 Liquid Rocket Engine, 4 November 1998, © NASA

LREs, despite their complexity, expensive manufacturing, and fuel cost, are the most powerful and reliable types of engines with I_{sp} reaching from 250-350 second range [5]. These will be our best possible engines in terms of raw power and efficiency until a better alternative is designed in the future. Modern LREs use various combinations of fuel and oxidizers, from traditional high efficiency liquid oxygen and liquid hydrogen (LOX/LH₂) combinations to hypergolic fuels which ignite upon contact with each other and are notoriously toxic. Famous oxidizer and fuel combinations are liquid oxygen and methane (LOX/CH₄), liquid oxygen and aviation grade kerosene (LOX/RP-1), 70% hydrogen peroxide and aviation grade kerosene (H₂O₂/RP-1) among others [3]. Another big component in determining the performance of LREs is the fuel combination, as not all have the same combustion output or produce the same I_{sp} .

1.3.1 Structure

Like most rocket engines, there are components which are integral for the operation and exist without exception in all archetypes of rocket engines. LREs, due to their complex design and amount of stored fuel on board of the rocket, have additional components besides the

mandatory combustion chamber, nozzle, and fuel tanks. These components are used to pump the fuel and oxidizers from the propellant tanks into the combustion chamber as well as to heat up the cryogenic fuel to a higher temperature to obtain optimal combustion. The drawing in Figure 7 below shows the two views of the man-rated, throttleable, reusable Space Shuttle main engine an LRE [3].

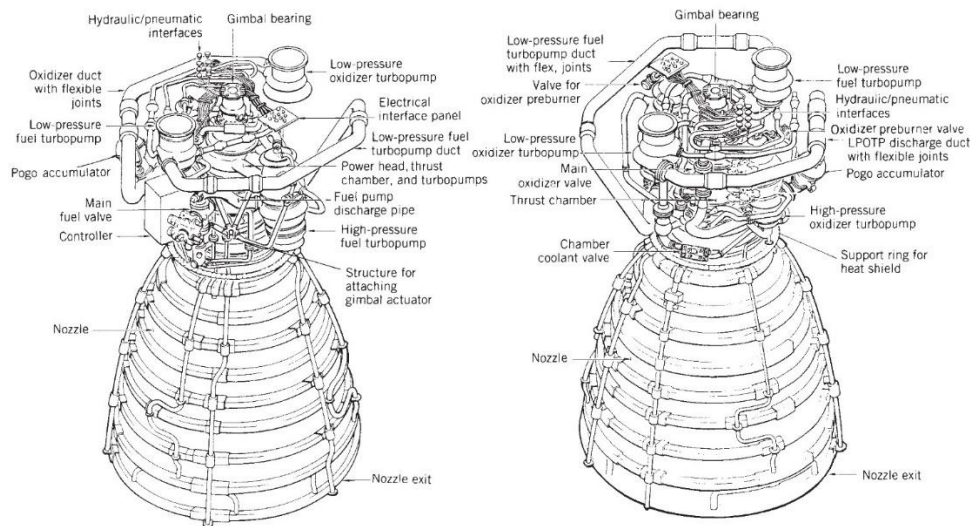


Figure 7: RS-25 Structural View, [3]

As can be seen in Figure 7 there are various additional components which were not present in SRM construction such as the oxidizer control valve, the high/low pressure oxidizer and fuel turbopumps, power heads, gimbal actuator structures, etc. The complexity of LRE construction also lies in the fact that various designs employ and exclude some components. The minimal required components for a common LRE's functionality are a combustion chamber, a nozzle, an injector, fuel/oxidizer tanks, and a propellant delivery system. Some designs opt for the use of turbopumps to deliver the fuel and oxidizer, while others use electric pump systems. The list below will discuss the most common LRE structural and functional components.

Common LRE Components:

- Turbopumps, pressure fed, or electrical fuel delivery systems.
- Primary and secondary combustion chambers.
- Gimble attachment structure for thrust vector control.
- Large De Laval bell nozzles.
- Pressure reducers and throttling valves.

- Chamber coolant valves and cooling systems.

There are different styles of fuel delivery systems all of which are used in LRE design, however, one of the most common types of fuel delivery systems are turbopumps. Turbopump propellant delivery systems utilize the ongoing propellant combustion within a secondary combustion chamber (also known as a gas generator) [5] in order to spin up fuel and oxidizer impellers. These impellers act as a pump drawing the fuel and oxidizer at the right pressure and mass flowrate into the primary combustion chamber, completing a cycle which can run indefinitely (until exhaustion of the fuel and/or oxidizer) without any continuous or semicontinuous intervention. An example of an LRE with turbopump propellant delivery systems can be seen in Figure 8 as a functional diagram.

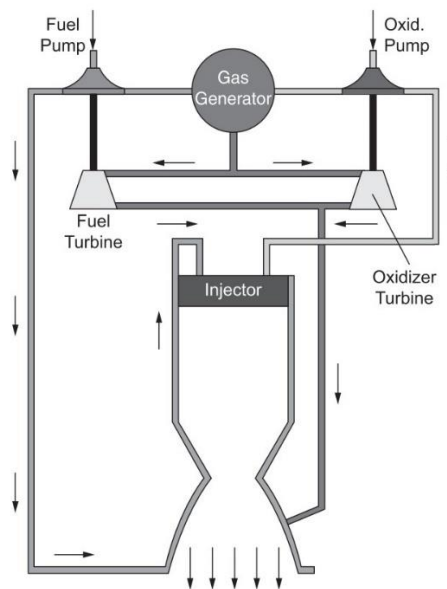


Figure 8: Functional Diagram of Liquid Rocket Engines with Turbopumps [5]

Other examples of fuel delivery systems are also widely used. In amateur or university-level LRE projects, pressure-fed fuel delivery systems are often used due to their ease of construction compared to turbopump delivery systems. In these systems the tanks holding the fuel and oxidizer are pressurized to a specific pressure. This allows the propellants to easily flow into the combustion chamber at the right flowrate simply by opening the valves. Details on other components of LREs are highly complex in their explanation and use practices and are of no

use to the main subject of this paper, therefore any further detailed discussion is not considered on the matter.

1.3.3 Advantages and Disadvantages

Being complex machines, LREs require near-ideal conditions and precise manufacturing to operate reliably and without hazard. There are many ways in which these engines can succumb to failure, an example of which is China's biggest rocket Long March 5 on June 2nd, 2017, causing failure of a mission to supply new and expensive military satellites into orbit. Despite the possibility of catastrophic scenarios, LREs still have many advantages compared to other types of rocket engines. The following list will name a few of both advantages and disadvantages of LREs.

Advantages

- High I_{sp} – compared to HREs
- High thrust – LREs can produce enough thrust to propel large rockets with heavy payloads like satellites, shuttles, structural modules for space stations, etc.
- Ability to throttle – this is one of the essential advantages LREs carry over other types of engines.
- Ability to be reignited – compared to SRMs, LREs can be shut down and powered back on at any time given there is sufficient fuel and oxidizer on board the rocket. This makes them excellent candidates for missions where engines need to be shut off and turned back on more than once (an example of this is the lunar descent and ascent modules of the Apollo missions)

Disadvantages

- Sensitive to vibrations, shock, and impacts – these engines are very sensitive to external disturbances as they have many intricate components which can fail during exposure to vibrations and/or shock.

- Need for large amounts of propellants – the propellants used by LREs are usually very combustible and produce a lot of energy. Often large volumes of fuel and oxidizer are used to satisfy the burn time requirement for these engines demand.
- Complexity – LREs are very complex in their design, often comprised of multiple subsystems of components which work together to produce the high amounts of thrust and provide a high I_{sp} .
- Use of cryogenic or toxic fuels and oxidizers – these types of propellants require specific design to make sure everything operates smoothly.

1.4 Hybrid Rocket Engines

1.4.1 HRE History and Applications

Hybrid Rocket Engines (HREs) are a type of rocket engine that operates by igniting a solid phase fuel and a liquid or gaseous phase oxidizer to produce thrust. These engines are considered the middle ground between the previously discussed rocket engine types as they are more efficient and functionally diverse than SRMs, but much simpler in construction than LREs. In the past some of these engines could not achieve an advanced technological readiness due to shortcomings, which hindered the establishment of these types of engines in the commercial space market [10]. HREs have a long history dating back to the 1930s, but it was not until the 1960s and 1970s that they began to be seriously investigated for use in spaceflight applications. Hybrid rocket engines offer several benefits over traditional solid or liquid rocket engines, including the ability to be throttled, or controlled, in a way that is not possible with SRMs. This makes HREs particularly attractive for use in space launch vehicles, where the ability to control thrust is critical for accurate trajectory control. In recent years, HREs have been used in a variety of systems, including the SpaceShipOne suborbital spacecraft, and the SpaceShipTwo reusable launch system (see Figure 9-a and Figure 9-b). HREs are also used in sounding rockets and experimental aircraft, as well as for suborbital and orbital launches [11].



Figure 9a: SpaceShipOne Suborbital System, Source (© Scaled Composites)



Figure 9b: SpaceShipTwo Reusable Launch System, Source (© Virgin Galactic)

Despite the progress that has been made in the development of HREs, there are still many challenges that need to be addressed to make them a practical and reliable option for use in space launch vehicles. For example, more work needs to be done to improve the safety and reliability of these systems, and to reduce the cost of producing and launching hybrid rocket engines [12]. Another key challenge in the development of these engines has been finding materials that are suitable for use as the solid fuel. Many of the materials that have been tested, such as rubber and plastics, have not been durable enough for use in long-duration flights. As a result, researchers have focused on developing more advanced materials, such as polymer-based fuels and composite materials, that are more suitable for use in HREs [13].

Overall, hybrid rocket engines have the potential to revolutionize the way we access space, offering a more flexible and cost-effective means of reaching orbit. As research and development in this area continues, it is likely that we will see even more exciting advances in the use of HREs in the coming years.

1.4.2 Structure

The basic structure of a HRE consists of four main components: the fuel grain, the injector, the combustion chamber, and the nozzle [14]. The fuel grain is the solid fuel used in the engine and is typically made of a material such as rubber, hydroxyl-terminated polybutadiene (HTPB), or polyethylene [15]. It is moulded into the desired shape and size for the particular application and is encased in a casing or liner to contain the fuel and protect it from the high temperatures and pressures of the combustion process [16]. Fuel grains come in different geometries which

have an effect that is tangential to that of SRMs (see Section 1.2.2). It determines the thrust profile and burn length of the engine. For the case of HREs this profile is true when the thrust is not being throttled.

The injector, unlike in LREs, is responsible for atomization of the oxidizer propellant and injection into the combustion chamber. It consists of nozzles and ports which propel the streams in such a way that they collide with each other and break off into particles small enough for optimal combustion [14]. Since the fuel in an HRE is in a solid phase, the fineness of the particles and the injected stream shape are what dictate the homogeneity of the propellant mixture and the efficiency of the combustion.

The combustion chamber is where the fuel and oxidizer are ignited and exhausted through the nozzle to create thrust. The chamber is typically made of a high-strength, heat-resistant material such as stainless steel or Inconel, and is designed to withstand the high temperatures and pressures of the combustion [15]. The combustion chamber length, and diameter are critical characteristics which determine most other parameters of the engine, including the thrust output.

The nozzle, as in all the previously described engines, is the final component of the HRE and is responsible for expanding and accelerating the hot gases produced by the combustion process to produce thrust. The nozzle typically consists of a converging section and a diverging section, and is designed to maximize the expansion of the gases and the conversion of thermal energy into kinetic energy [16].

In comparison to LREs, HREs have a less complex and less expensive structure, however, they still provide benefits such as being able to be throttled and shutdown and powered back on multiple times given there is enough fuel and oxidizer remaining. Please see Figure 10 for visual aid on the internal structure of an HRE.

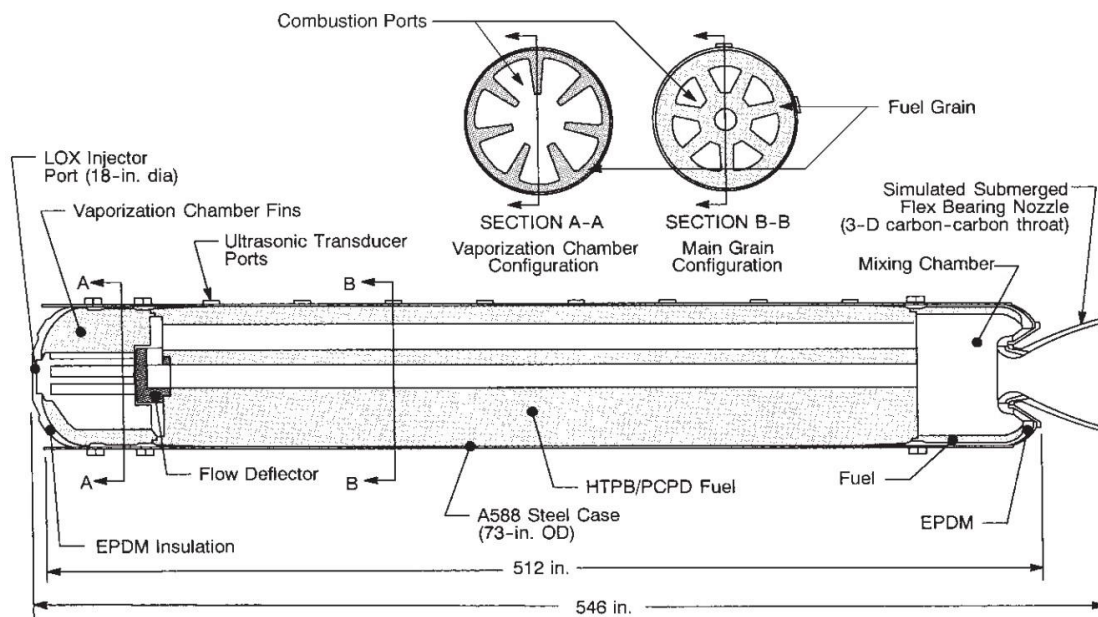


Figure 10: Hybrid Rocket Engine Internal Structure, [3]

1.4.3 Advantages and Disadvantages

When comparing HREs to SRMs and LREs, several distinct advantages and disadvantages can be noted with regards to operation and use. Be it simplicity, cost, or material costs, HREs are arguably one of the best solutions for many tasks in the aerospace field, where cost efficiency and good performance are of importance. The following two lists discuss the advantages and disadvantages of HREs in greater detail. All references for the items in the lists below are procured from the following reference [17] .

Advantages

- Simplicity – HREs are simpler in design and have fewer moving parts compared to liquid rocket engines, which can make them easier to manufacture and maintain.
- Throttling HREs can be easily throttled, or adjusted to produce different thrust levels, which allows for greater control during flight.

- Versatility – Hybrid rocket engines can be used for a variety of applications, including suborbital and orbital spaceflight, as well as for launching small payloads into space.
- Cost – HREs are generally less expensive to manufacture than LREs, as they do not require complex pumps and other mechanical components.
- Reliability – HREs have a high level of reliability due to their simple design and lack of moving parts, which can make them a good choice for space missions that require a high level of reliability.
- Performance – HREs can achieve high specific impulse, or the amount of thrust produced per unit of fuel, which can make them more efficient than solid rocket engines.
- Environmental friendliness – HREs typically produce lower levels of toxic and carcinogenic emissions compared to SRMs, which can make them more environmentally friendly.

Disadvantages

- Performance – Hybrid rocket engines may not be as powerful as LREs, which can limit their use in certain applications.
- Throttling – The ability to throttle HREs may be limited, as the fuel grain must be designed to burn at a specific rate.
- Environmental friendliness – Hybrid rocket engines may produce more emissions than LREs, as they rely on the combustion of solid fuel.
- Throttling – Hybrid rocket engines may not be able to throttle as quickly as liquid rocket engines, as the fuel grain must be designed to burn at a specific rate.
- Restartability – Hybrid rocket engines may not be able to restart once they have been shut down, as the solid fuel cannot be easily restarted once it has been ignited.
- O/F Shift – During operation because of solid fuel regression, the ratio between oxidizer and fuel mass flowrates changes resulting in a decrease in the specific impulse of the engine.

Given the lists above, it can be said that HREs have most of the necessary benefits to be used in the space industry, if the inefficiencies can be reduced to at least match those of LREs.

1.5 Aim of the Study

The focus of this paper is on improving the efficiency (I_{sp}) of HREs by utilizing control methodologies. One of the main disadvantages as stated in Section 1.4.3 is the shift of the OF ratio during operation. This is caused by fuel regression which over time increases the combustion surface area causing more fuel per unit of time to be vaporized and ignited in the combustion chamber. The increase of the mass flowrate of the fuel causes the ratio of oxidizer and fuel mass flowrates to shift, making the mixture in the chamber fuel rich. Shifts in OF ratio impact the efficiency due to insufficient combustion which lowers the I_{sp} . During incomplete combustion not all particles of the fuel are burned as there is not enough oxidizer supplied into the chamber to accommodate for the increased fuel flowrate. This process is visualized by Figure 11 taken from a paper on Dynamic Numerical Simulation of Hybrid Rocket Moto with HTPB-Based Fuel by H. Tian et al [18] below where an I_{sp} vs OF ratio graph is drawn.

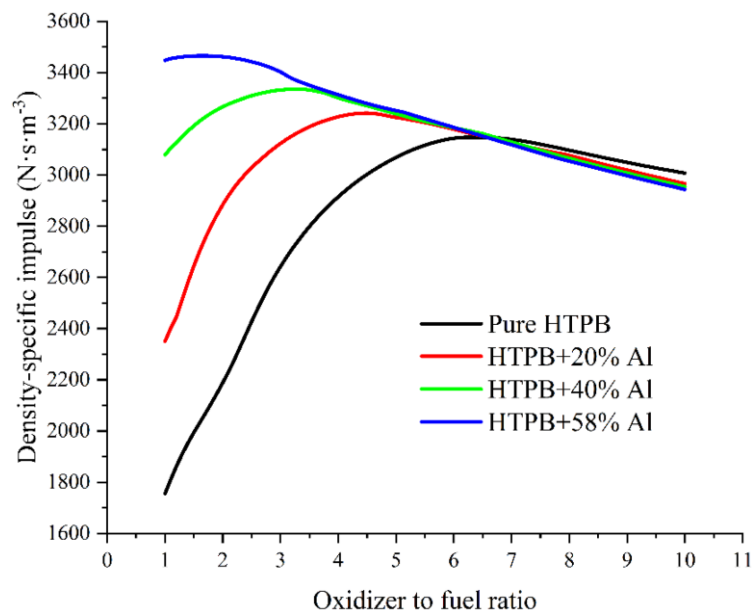


Figure 11: Specific Impulse vs OF Ratio graph [18]

The approach of this paper is to introduce an HRE design which accounts for the increase in fuel mass flowrate over time. The governing differential equations of the HRE system will be formulated and an appropriate controller will be designed which will interpolate the proportionality of shifts in OF ratio throughout the time of combustion. The designed controller will either increase or decrease the mass flowrate of oxidizer based on the current state of the system, which will improve the combustion and increase the I_{sp} .

2.0 Theory and Mathematical Preliminaries

2.1 General Equations

During combustion and operation of the HRE and most rocket engines variables change in primarily one axis along the combustion chamber. The flow of gases in this case can be considered as quasi-one-dimensional (by definition). This allows to assume that there is no flow in any other axes. While in real rocket flow is not isentropic, however, this is a simplification of the flow for the purpose of modelling and is reasonably close to real life observations. Therefore, we can consider the final flow we will be working with to be Quasi-one-dimensional Isentropic Flow, and therefore a conclusion can be made that this thermodynamic process has no heat transfer. Finally, we can consider that our process is Adiabatic, and all flow is assumed to exist only along the axis of revolution of the combustion chamber.

The thrust of a rocket engine can be generalized by the standard formula below [3]:

$$F = \dot{m}v_e + (P_{atm} - P_e)A_e \quad (2-1)$$

\dot{m} – mass flow rate of exhaust gases

v_e – exit velocity of exhaust gases

P_{atm} – atmospheric pressure

P_e – exit pressure of exhaust gases

A_e – exit area of the nozzle

By considering an ideal nozzle, when $P_e = P_{atm}$ we can simplify the formula further:

$$F = \dot{m}v_e \quad (2-2)$$

To calculate the Total Impulse (hereafter I_t), we simply integrate Eq. (2-2) over time getting the following:

$$I_t = \int_0^t F dt = \int_0^t \dot{m}v_e dt \quad (2-3)$$

The mass flow rate \dot{m} is the numeric summation of the mass flow rate of the oxidizer (\dot{m}_{ox}), and the mass flow rate of the fuel (\dot{m}_f). See Ref. [3].

$$\dot{m} = \dot{m}_{ox} + \dot{m}_f \quad (2-4)$$

Of Specific Impulse, we know that it equals the Total Impulse defined in Eq. (2-3) over the total mass of the propellant burned times g (free fall acceleration) and utilizing Eq. (2-4) we get the following.

$$I_{sp} = \frac{I_t}{(\dot{m}_f + \dot{m}_{ox})g} = \frac{\int_0^t \dot{m}v_e dt}{(\dot{m}_f + \dot{m}_{ox})g} \quad (2-5)$$

As defined in Ref [3] , mixture ratio (**OF** ratio) is defined with the following formula.

$$OF = \frac{\dot{m}_{ox}}{\dot{m}_f} \quad (2-6)$$

From Eq. (2-5) and Eq. (2-6) we can say that

$$\dot{m} = \dot{m}_{ox} + \dot{m}_f = \dot{m}_f(OF + 1) \quad (2-7)$$

We need to take into account the regression of the fuel grain radius throughout the burn, which as per Ref. [5] the regression rate is influenced by port oxidizer mass flux G . We can observe the general formula below, where a and n are empirically found constants.

$$\dot{r} = aG_{ox}^n = a \left(\frac{\dot{m}_{ox}}{A_p} \right)^n \quad (2-8)$$

A_p – port area

The port area and burn surface area (A_b) can be further defined geometrically by the time-dependent port radius $R(t)$.

$$A_p = \pi R^2 ; A_b = 2\pi RL \quad (2-9)$$

A_b – surface burn area

L – combustion chamber length

From Eq. (2-8) and Eq. (2-9) we can say that.

$$\dot{r} = a \left(\frac{\dot{m}_{ox}}{A_p} \right)^n = a \left(\frac{\dot{m}_{ox}}{\pi R^2} \right)^n \quad (2-10)$$

Looking at Eq. (2-10), if \dot{m}_{ox} is kept constant (which holds true for many designs during standard non-throttling operations) than regression rate $\dot{r} \propto R^{-2n}$ [5]. According to the same reference and the results of Eq. (2-10), when R grows, the regression rate will decrease, which is true for all HREs. Utilizing these findings, the expression for fuel mass flow rate can be written as follows.

$$\dot{m}_f = \dot{r} \rho_f A_b = a \rho_f \left(\frac{\dot{m}_{ox}}{\pi R^2} \right)^n 2\pi R L = 2a \pi^{1-n} \rho_f L \dot{m}_{ox}^n R^{1-2n} \quad (2-11)$$

ρ_f – solid phase fuel density

From Eq. (2-11) we can then conclude that $\dot{m}_f \propto R^{1-2n}$. Knowing the definition of regression rate as being the change of radius over time we can find the Eq. of time-dependent radius $R(t)$.

$$\dot{r} = \frac{dR}{dt} = a \left(\frac{\dot{m}_{ox}}{\pi} \right)^n R^{-2n} \quad (2-12)$$

Looking at Eq. (2-12) we can see that we have a separable differential equation. By separating the variables, we get Eq. (2-13) and by integrating both sides we get Eq. (2-14).

$$R^{2n} dR = a \left(\frac{\dot{m}_{ox}}{\pi} \right)^n dt \quad (2-13)$$

$$R(t) = \left[a(2n + 1) \left(\frac{\dot{m}_{ox}}{\pi} \right)^n t + R_0^{2n+1} \right]^{\frac{1}{2n+1}} \quad (2-14)$$

R_0 – initial radius of fuel port

Finally, utilizing Eq. (2-11) and Eq. (2-14) we get the fuel mass flow rate history given by Eq. (2-15).

$$\dot{m}_f(t) = 2a\pi^{1-n}\rho_f L \dot{m}_{ox}^n \left[a(2n + 1) \left(\frac{\dot{m}_{ox}}{\pi} \right)^n t + R_0^{2n+1} \right]^{\frac{1-2n}{1+2n}} \quad (2-15)$$

As stated in Ref. [5] and can be observed in Eq. (2-15), we can understand that \dot{m}_f is constant when $n=0.5$ and that for numbers of $n>0.5$ our mass flowrate of the fuel will decrease with time which from Eq. (2-6) will mean that **OF** will increase with time diminishing the Isp of the HRE.

2.2 Engine and Fuel Parameters

To perform the simulations, before the introduction of any type of control, an engine design is needed to model the L and R_0 parameters from Eq. (2-15) which we have covered in Chapter 2.1. The HYDRA 3X student-built hybrid rocket engine [10] (Figure 12) was chosen for the purpose of modelling the equations that are needed.

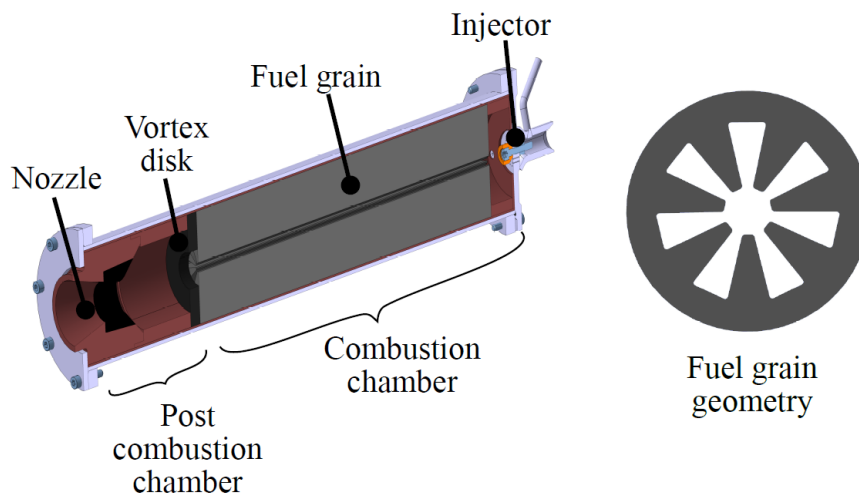


Figure 12: Design of HYDRA 3X Hybrid Rocket Engine [10]

For the purposes of this research the throat diameter was taken as R_0 as a cylindrical grain geometry was assumed in the calculations. All calculations discussed in Chapter 3.0 will be

calibrated using the max peak thrust, specific impulse, and other useful information. In Figure 13 below you can see the parameters provided by F. Heeg et al [10].

Parameter	Symbol	HYDRA 3X	HYDRA 4X
Overall length	l	0.47 m	0.62 m
Overall diameter	d	0.09 m	0.14 m
Fuel grain length	l_f	0.31 m	0.34 m
Post combustion chamber length	l_{post}	0.05 m	0.10 m
Nozzle throat diameter	d_t	0.02 m	0.03 m
Nozzle area ratio	A_e / A_t	5.06	4.97
Mass	m	5.7 kg	5.78 kg
Fuel mass	m_f	1.2 kg	2.57 kg
Casing mass	m_{cas}	3.8 kg	0.31 kg
Thrust	F	1.25 kN	2.25 kN *
Total impulse	I_{tot}	12.5 kNs	35.55 kNs *
Chamber pressure	p_c	3 MPa	2.5 MPa *

* Design value.

Figure 13: Structural and performance characteristics of the engines HYDRA 3X and 4X [10]

Furthermore, to come up with a generalized control equation that can work for different fuel types, burn rate variation from fuel to fuel need to be considered. From the conclusions of Chapter 2.1, specifically Eq. (1-12), it is known that different types of fuel result in a different regression rate, which in turn changes the behaviour of $\dot{m}_f(t)$ based on the Regression Rate Coefficient - \mathbf{a} and Flux Exponent - \mathbf{n} . For this reason, regression rate data for multiple fuel types (14 in total) was used to investigate the behaviour of the developed control equations for different fuel types. The data was taken from a paper on Hybrid Rocket Engine Regression Rate Data and Modelling by authors G. G. Zilliac and A. Karabeyoglu [19]. In Figure 14 below the used regression rate test data can be seen, taken from the source mentioned above.

Results summary of the average regression rate with oxygen for various fuels									
No.	Fuel	a^\dagger	n	No. of Tests	Chamber Pressure Range (MPa)	Average O/F Ratio Range	Data Reduction Technique	Oxidizer Mass Flux Range (g/cm ² -sec)	Ref.
1	Paraffin, SP1A	0.488	0.62	65	1.1-6.9	1.0-4.0	DA	1.6-36.9	15
2	HTPB, (Thiokol)	0.146	0.681	16	-	-	-	3.8-30.2	16
3	HTPB+19.7%AL	0.117	0.956	2	1.2	-	OA	5.1-23.0	17
4	HTPB	0.304	0.527	3	2.0	-	OA	6.2-31.0	17
5	HTPB+20%GAT	0.473	0.439	5	-	-	-	-	18
6	PMMA	0.087	0.615	8	0.3-2.6	-	-	3.3-26.6	19
7	HDPE	0.132	0.498	4	0.7-1.3	3.8-5.9	DA	7.7-26.1	20
8	PE Wax, Marcus 200	0.188	0.781	4	0.5-1.2	2.2-3.2	DA	4.8-15.8	20
9	PE Wax, Polyflo 200	0.134	0.703	3	0.6-1.2	1.6-1.7	DA	4.4-16.3	20
10	HTPB	0.194	0.670	6	-	-	OA	17.5-32.0	21
11	HTPB+13% nano Al	0.145	0.775	12	-	-	OA	16.5-34.2	21
12	Paraffin, FR5560 + 13% nano Al	0.602	0.730	8	-	-	OA	14.5-29.0	21
13	Paraffin, FR5560	0.672	0.600	4	-	-	OA	6.3-12.3	21
14	Paraffin, FR4550	0.427	0.748	3	0.7-?	1.3-1.8	DA	4.3-11.9	20

Regression rate equation: $\bar{r} = a\bar{G}_o^n x^m$ with $m = 0$

[†] For use with G_o with units of gm/cm²-sec, produces an average regression rate in mm/sec.

DA: Diameter Averaged, FA: Flux Averaged, AA: Area Average, OA: Other averaging technique applied

Figure 14: Regression Rate Test Data [19]

3.0 Results and Discussion

3.1 Mathematical Framework

The proposed method of control requires controlling the oxidizer valve to decrease or increase \dot{m}_{ox} proportional to $\dot{m}_f(t)$ function. For this we need to first derive the oxidizer mass flowrate control equation. This is done by taking the fuel mass flowrate history function given by Eq. (2-15) and substituting \dot{m}_f expressed from Eq. (2-6). This gives us the following.

$$\dot{m}_{ox}/OF = 2a\pi^{1-n}\rho_f L\dot{m}_{ox}^n \left[a(2n+1) \left(\frac{\dot{m}_{ox}}{\pi} \right)^n t + R_0^{2n+1} \right]^{\frac{1-2n}{1+2n}} \quad (3-1)$$

If we then multiply both sides of Eq. (3-1) by **OF** we get the preliminary form of our control function.

$$\dot{m}_{ox} = \left(2a\pi^{1-n}\rho_f L\dot{m}_{ox}^n \left[a(2n+1) \left(\frac{\dot{m}_{ox}}{\pi} \right)^n t + R_0^{2n+1} \right]^{\frac{1-2n}{1+2n}} \right) OF \quad (3-2)$$

We can further simplify Eq. (3-2) by gathering the similar terms on the right-hand side and rewriting the function which can then be solved with respect to \dot{m}_{ox} .

$$\left(a\pi^{1-n}\rho_f L\dot{m}_{ox}^{n-1} \left[a(2n+1) \left(\frac{\dot{m}_{ox}}{\pi} \right)^n t + R_0^{2n+1} \right]^{\frac{1-2n}{1+2n}} \right) OF = 1 \quad (3-3)$$

Due to the varying fuel parameters n and a we are unable to solve this equation analytically, which complicates the derivation of a control equation as it must be solvable in a non-numeric manner such that it does not require a lot of computing power when it is used practically with an on-board computer. For this reason, the function must be first solved numerically for the 14 types of fuels used in this study, and then approximated by a different function which can be solved analytically. MATLAB R2022a (MathWorks Inc.) was used for all the calculations and simulations moving forward and the derived control function (hereafter Theoretical Control Function or TCF) given by Eq. (2-3) was solved numerically using the *vpasolve()* numerical

solver. The plots with respect to time of the TCF for all 14 propellant types can be seen in Figure 15 below.

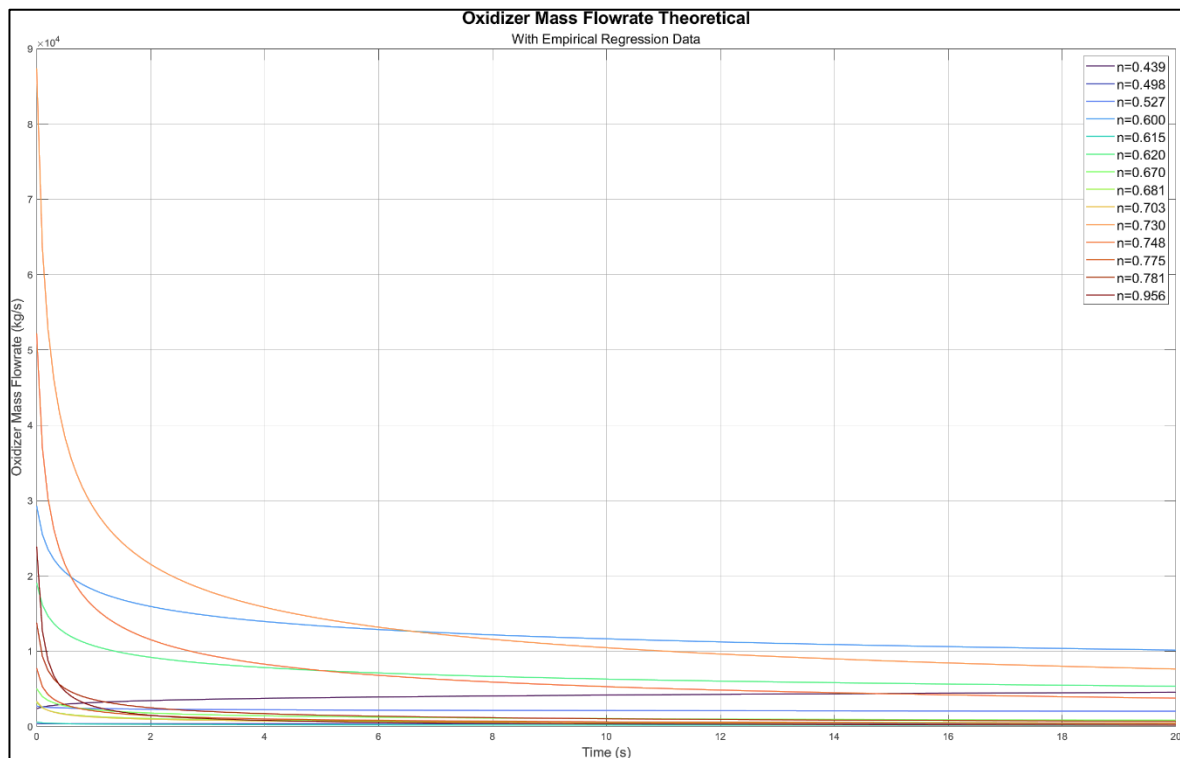


Figure 15: Theoretical Control Function (TCF)

We now know what our TCF must look like for each type of propellant used in this study, which provides the first step in creating a generalized Control Function that can be used for all propellant cases. To get to that goal, however, we need to first address some of the immediately apparent issues of the TCF.

Firstly, it is apparent both visually, and confirmed by the values of the numerical approximation, that at $t = 0 \text{ s}$ we would need infinite \dot{m}_{ox} to control the engine. Since this is physically impossible, we can combat this event by approximating the increase of mass flowrate from when the engine is being ignited by modelling an increasing function up to some time t_{int} ¹ (will be covered in Chapter 3.2.4 in greater detail.)

Secondly, Eq. (3-3) is the only way to find the control equation we have as of now, and it is impossible to do analytically.

¹ t_{int} – the time to which we simulate the effect of the valve opening upon the startup of the engine.

An alternative approach to finding the control function from the TCF, is to take the generated output for each fuel, and perform fittings to approximate it with a time-dependent equation with the fuel parameters \mathbf{n} and \mathbf{a} , such that it is applicable for each case of fuel and can closely follow the values of the TCF. Chapter 3.2 will focus on 3 primary methods of approximating the control function, analysing the advantages, disadvantages and challenges that were faced during the process.

3.2 Mathematical Approximations

The following chapter will discuss three methods of modelling the analytical control function. The methods were done using the Curve Fitter application in MATLAB and the Non-linear Fitting Analysis tool in Origin Pro.

3.2.1 Exponential Fitting (*MATLAB Curve Fitter*)

The initial approach was to model the control equation as an exponential function. Fittings with a single exponent did not result in sufficiently high R^2 value, which is why the TCF was fitted using a sum of two exponents given in the equation below.

$$\dot{m}_{ox}(t)^{*2} = k_1 e^{q_1 t} + k_2 e^{q_2 t}$$

t – time (s) (3-4)

$k_{1,2}$ – multiplication coefficient

$q_{1,2}$ – exponent coefficient

The procedure was repeated for the entire set of theoretical values which can be seen in Chapter 3.1 Figure 15. See Figures 16-a and 16-b below for an example of the fitting process for one of the fuels with the plot vs time, residuals plot and confidence interval.

² * –indicates an approximated function and will be used for that purpose moving forward in the paper.

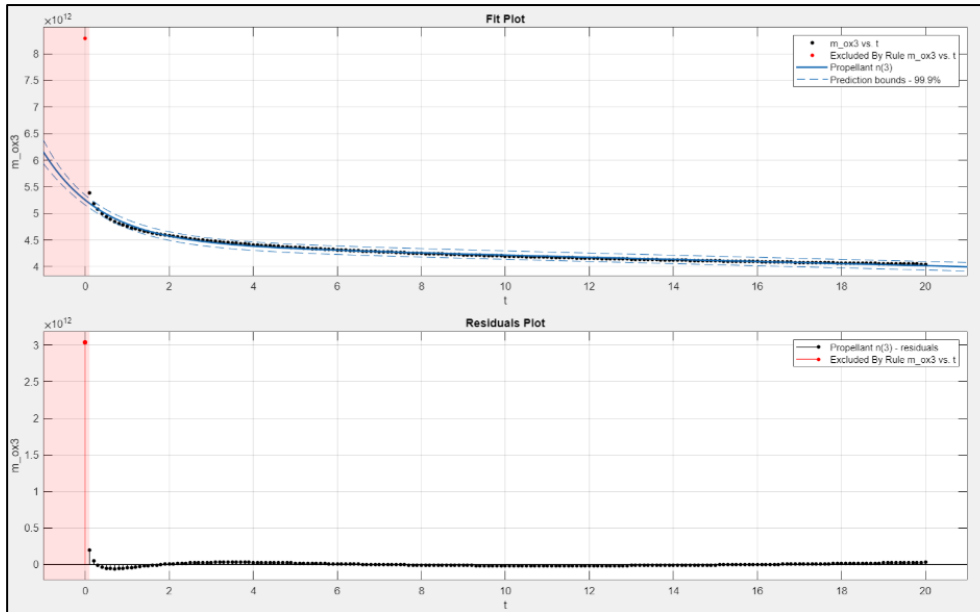


Figure 16-a : Exponential fitting \dot{m}_{ox} with $n = 0.527$

The results of the coefficients for the fitting can be seen in Figure 16-b below.

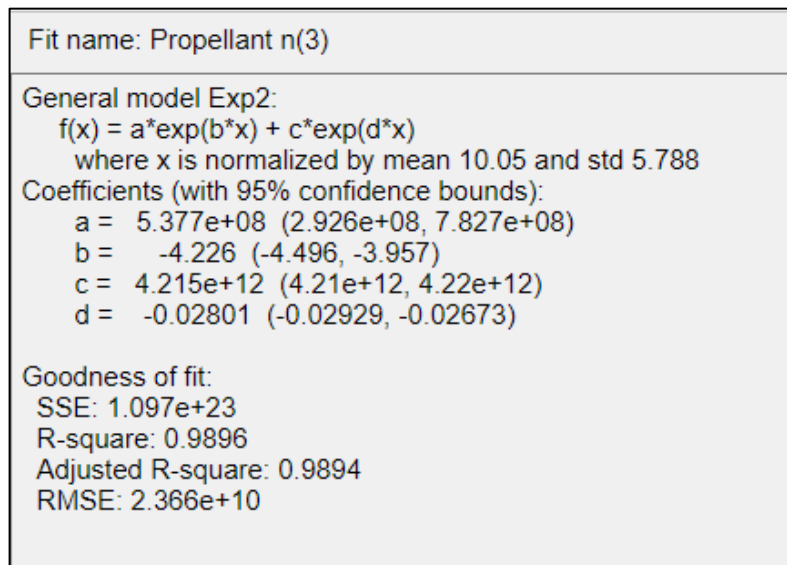


Figure 16-b : Exponential Approximation Results Example

The fitting was repeated for all propellants except two which had the parameter $n < 0.5$, resulting in an average $R^2 = 0.9789$ which was considered satisfactory for an initial fitting.

Now that we have the necessary coefficients k_1, q_1, k_2 and q_2 for the composite exponential fitting for each propellant respectively, the next step is to model each of the coefficients with

the regression parameters to find a generalized control equation. This was yet again performed in MATLAB using the Curve Fitting application. After fitting of each of these coefficients we find the following proportionalities.

$$k_1 \propto 4.023 * 10^6 n^{-7.8} \quad (3-5)$$

$$q_1 \propto (-0.7275)n^2 - (4.016)n - 9.244 \quad (3-6)$$

$$k_2 \propto 6.993 * 10^{13} a^{2.597} \quad (3-7)$$

$$q_2 \propto (-0.02804)n^2 - (0.1547)n - 0.2424 \quad (3-8)$$

Plugging the proportionalities for each coefficient into the exponential sum model shown in Eq. (3-4) we get the following generalized control equation.

$$\begin{aligned} \dot{m}_{ox}(t)^* = & (4.023 * 10^6 n^{-7.8}) e^{((-0.7275)n^2 - (4.016)n - 9.244)t} + \\ & + (6.993 * 10^{13} a^{2.597}) e^{((-0.02804)n^2 - (0.1547)n - 0.2424)t} \end{aligned} \quad (3-9)$$

a – Regression Rate Coefficient

n – Flux Exponent

Using Eq. (3-9), we are now able to approximate the TCF. As can be seen the function can be solved analytically, as all that is required to obtain the necessary \dot{m}_{ox} is to plug in the fuel parameters of choice and plot the function with respect to time. In Figure 17 below we can see the resulted plots of the Composite Exponential Control Function (CECF).

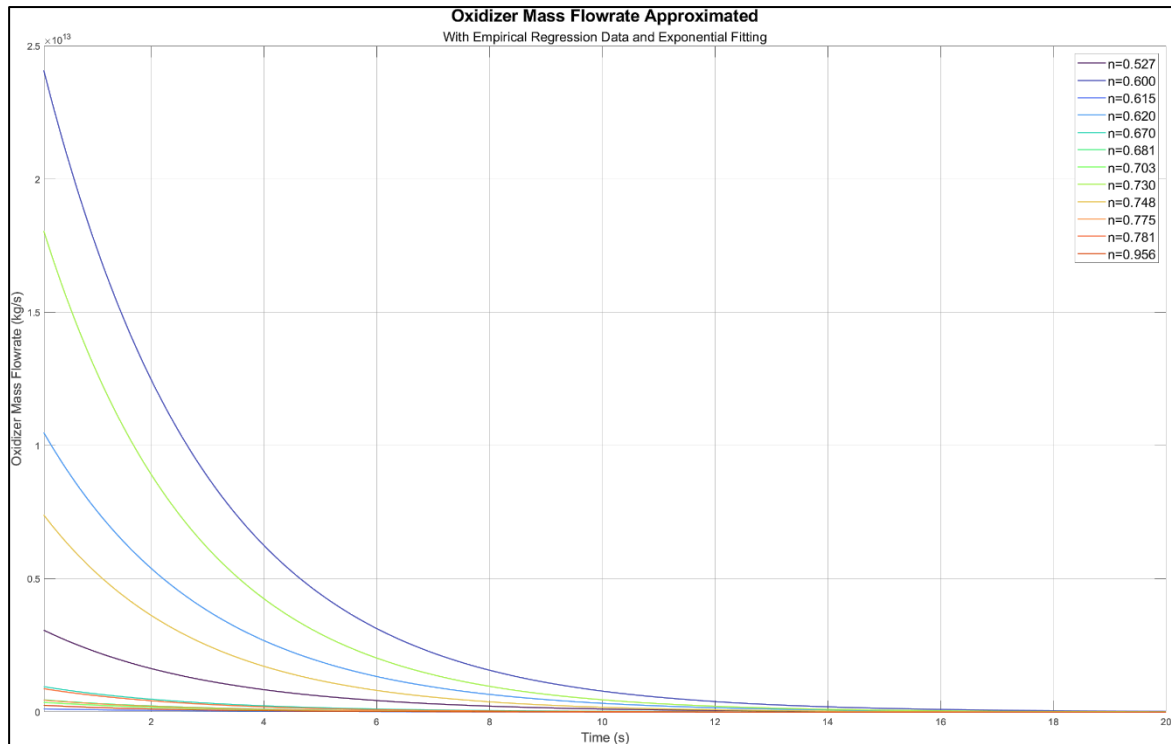


Figure 17: Composite Exponential Control Function (CECF)

Let us discuss the negative aspects of such an approximation. As we can see from the plots of the CECF, the values of \dot{m}_{ox} are grossly overestimated in amplitude by a factor of 10^9 . It is also clearly visible that the function converges to zero relatively quickly which is due to it being exponential. This is not optimal not only because of the overestimation of the values, but also for the reason of fast attenuation. Even if the values are calibrated to be proportional to those of the TCF, this control function would result in the engine shutting off during some time of operation due to the \dot{m}_{ox} being equal to zero (analogous to closing the oxidizer valve on the rocket). If calibrated, the CECF would be functional only for short burning engines, the burn-time of which does not exceed ~ 16 seconds. It is for this reason that this method of modelling the control function was considered unsatisfactory, although it could still (if made proportional the TCF values) be a functional open loop controller for short burning engines.

3.2.2 Power Fitting (*MATLAB Curve Fitter*)

From analysing the CECF and its downsides, we can now start constructing a better approximation to the TCF, taking into consideration that the control function needs to attenuate

to some $\dot{m}_{ox} \neq 0$ value to ensure that it can perform for engines with a large range of burn-times and not shut it off.

Let us examine the TCF closely. Looking back at Eq. (3-3) we can see that the very rough approximation of that function (as in without considering parameters like $L, \rho_f, etc.$) is a power function. Therefore, we can take an approximation as a power function given by the equation below.

$$\dot{m}_{ox}(t)^* = kt^q$$

$$t - \text{time (s)} \tag{3-10}$$

k – multiplication coefficient

q – exponent coefficient

Performing the same investigations as in Chapter 3.2.1, we perform the approximation using MATLAB's Curve Fitting application with respect to time, and then perform a fitting for the coefficients with the fuel parameters to get a generalized function. The regressions resulted in approximations with $R^2 = 0.9927$ on average which is already an increase from the CECF model.

Just like in the previous chapter we can see the plots of the power fitting for a single propellant type. Figure 18-a below will show a step from the fitting process for a single propellant including the plot vs time and the residuals plot with the confidence interval.

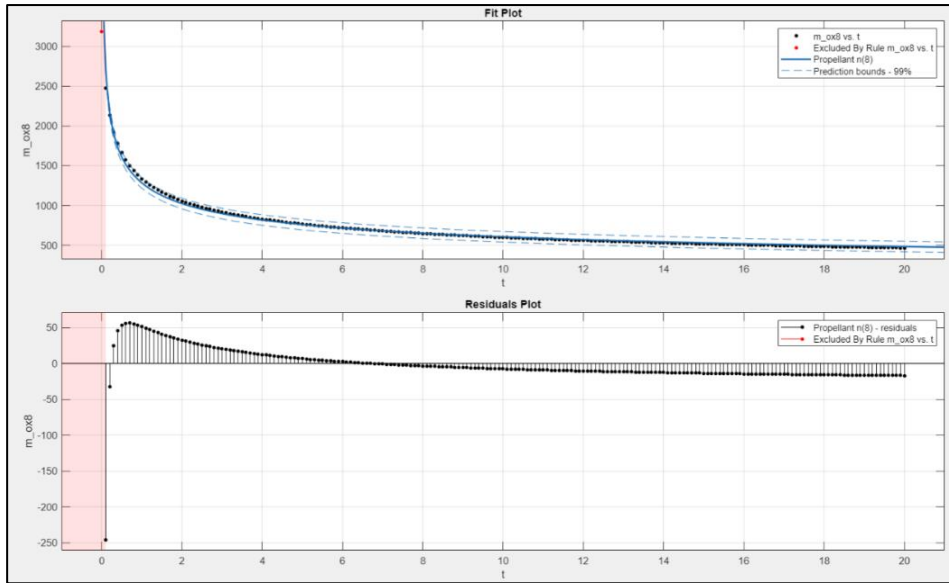


Figure 18-a: Power fitting \dot{m}_{ox} with $n = 0.681$

The results of the coefficients for the fitting can be seen in Figure 18-b below.

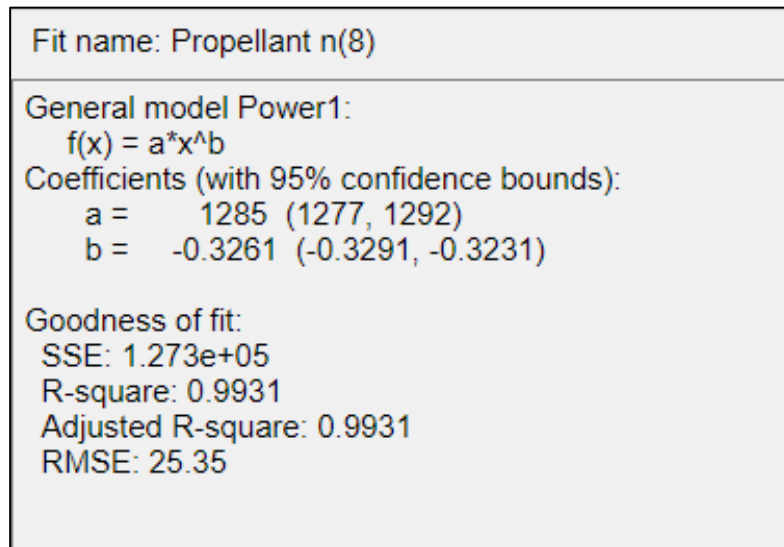


Figure 18-b: Power Approximation Results Example

We can see the resulting proportionalities of the coefficients and the fuel parameters after completing the coefficient fitting with respect to the fuel parameters in the equation below.

$$k \propto 2.896 * 10^4 a - 2531 \quad (3-11)$$

$$q \propto 0.8 - 1.6 * n \quad (3-12)$$

Now if we substitute the fittings of k and q into Eq. (3-10) we get a generalized control function which will approximate the numerically solved values of \dot{m}_{ox} .

$$\dot{m}_{ox}(t)^* = (2.896 * 10^4 * a - 2531)t^{(0.8-1.6n)} \quad (3-13)$$

Using Eq. (3-13), we are now able to approximate the TCF as a new control function which can be solved analytically. All that is required to obtain the necessary \dot{m}_{ox} is to plug in the fuel parameters of choice and plot the function with respect to time. In Figure 19 below we can see the resulted plots of the Power Control Function (PCF).

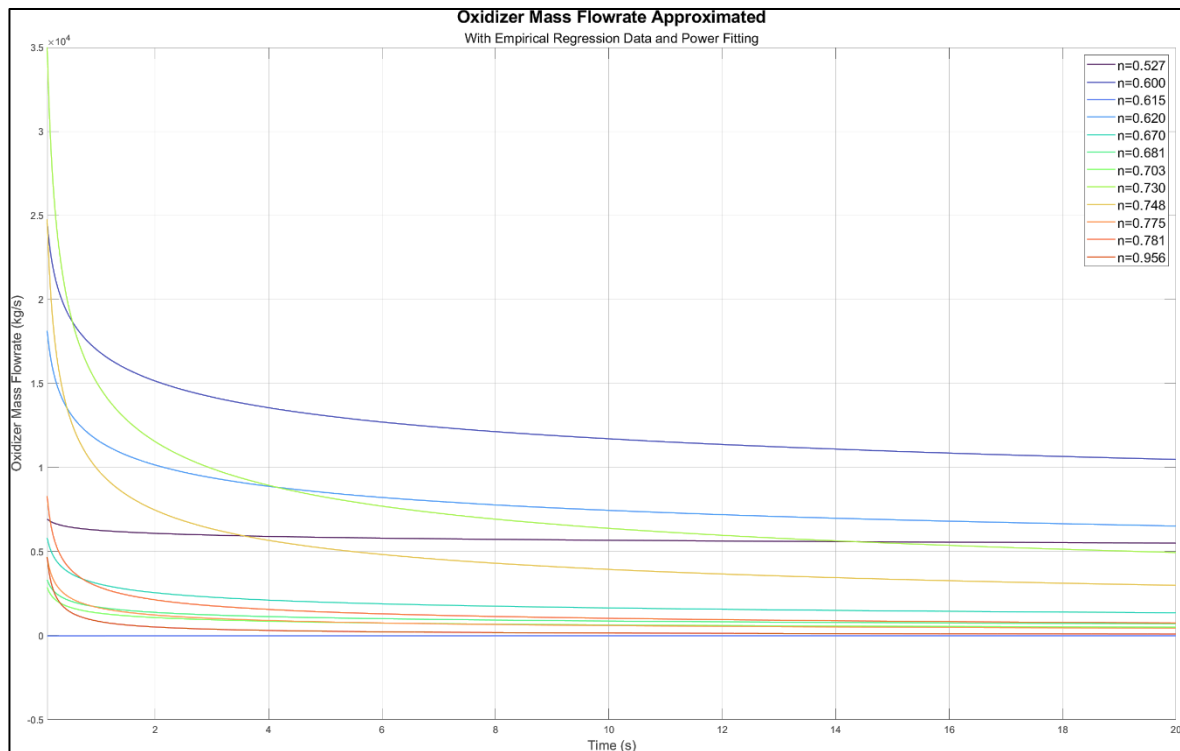


Figure 19: Power Control Function (PCF)

This control function, unlike the CECF, yields a closer result to the TCF both in amplitude and in the rate of attenuation. The amplitude of the PCF is three times less than the TCF which is still an inaccuracy. As for other drawbacks of this approximation, if we look at Eq. (3-13) we can see that in the event when $n > 0.5$ at $t = 0$ our \dot{m}_{ox} value tends to positive infinity. This is problematic for practical applications as such an input would result in windup of the digital

controller regulating the valve. Being close to the TCF values shows that the power fitting is a much better fit for our application, but also that further improvements are needed to make it functional.

3.2.3 Belehradek Power Fitting (*Origin Pro*)

To further improve the approximation of the TCF, specifically the \dot{m}_{ox} values tending to infinity at $t = 0$ s, a different power fitting must be considered. To take care of this issue, a different power fitting called the Belehradek Power Fitting was used. MATLAB Curve Fitter did not have the capability to readily perform such a fitting, which is why this fitting was performed using Origin Pro (Origin Lab Inc.). We will be approximating our control function according to the formula below.

$$\dot{m}_{ox}(t)^* = k(t - p)^q$$

t – time (3-14)
 k – multiplication coefficient
 q – exponent coefficient

As with the previous cases, each propellant type will be approximated after which the resulting coefficients will be modelled to find proportionalities with the fuel parameters. Unlike the previous cases, new theoretical \dot{m}_{ox} is calculated, once keeping the Regression Rate Coefficient a and varying the Flux exponent n from 0.5 to 1 with a step size of 0.0385, and once vice versa. This helps us ensure we find separate correlations between the parameters, and then combine the results to get a final control equation. Initially, the non-linear fitting tool in Origin Pro was used to fit the TCF outputs with respect to time, after which the coefficients are fitted with respect to the fuel parameters using the Curve Fitter in MATLAB. For the plots of the theoretical \dot{m}_{ox} with variable Flux Exponent the Regression Rate coefficient value was set to a constant $a = 0.473$ and for the plots with variable Regression Rate coefficient, the Flux Exponent value was set to a constant $n = 0.5$. In the Figures 20-a and 20-b below you can see the resulting plots of the Theoretical \dot{m}_{ox} with constant Regression Rate Coefficient and the Theoretical \dot{m}_{ox} with constant Flux Exponent both with respect to time.

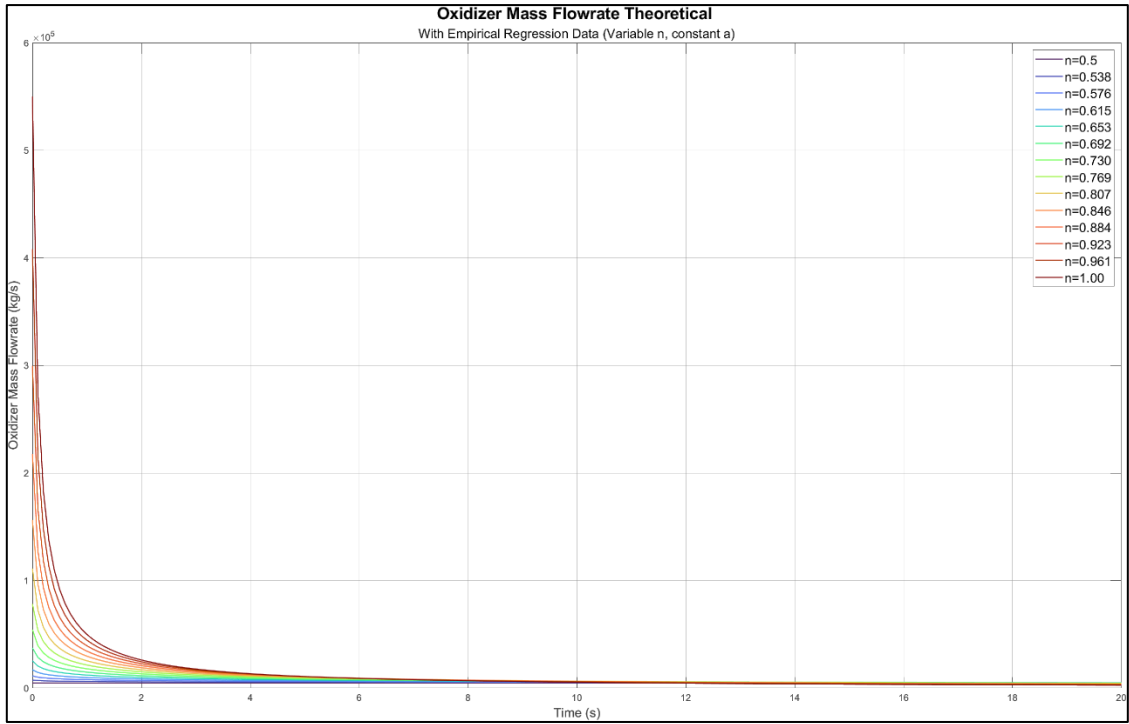


Figure 20-a: Theoretical \dot{m}_{ox} with variable Flux Exponent

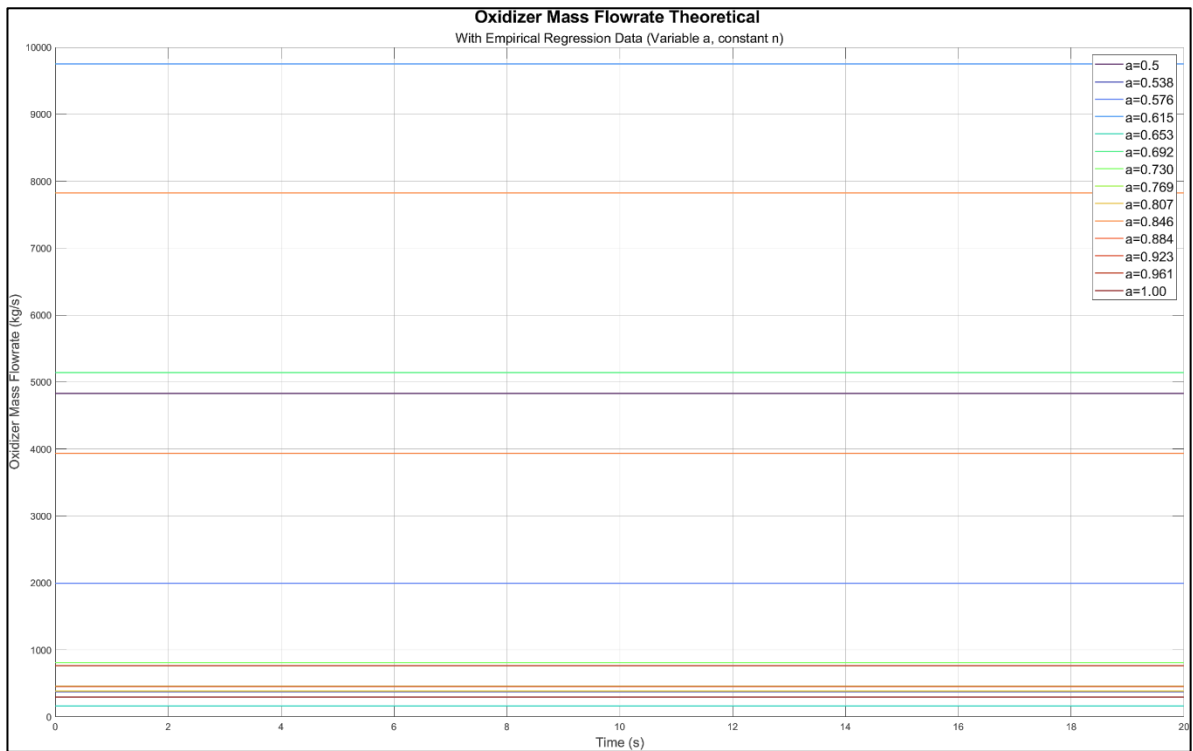


Figure 20-b: Theoretical \dot{m}_{ox} with variable Regression Rate Coefficient

The results from Figure 20-a were taken into Origin Pro and fitted using the Belehradek Power function. The fittings were performed for 7 iterations with respect to time per fuel on average

to reach a $R^2 = 1$ indicating a perfect fit for each of the propellants. The fitted values of coefficients were then written out and taken into MATLAB to be fitted with the fuel parameters. The values of all the coefficients for the 14 fuels can be seen in Table 1 below.

Table 1: Origin Pro Fitting Coefficients

Fuel Parameter (n)	k	p	q
0.5000	4830.71	-0.25658	0
0.5384	6236.63	-0.10001	-0.07692
0.5769	7957.31	-0.10001	-0.15385
0.6153	10034,69	-0.10000	-0.23077
0.6538	12508.66	-0.10000	-0.30769
0.6923	15414,70	-0.10000	-0.38462
0.7307	18781.32	-0.10000	-0.46154
0.7692	22627.34	-0.10000	-0.53846
0.8076	26959.18	-0.10000	-0.61538
0.8461	31768.37	-0.10000	-0.69231
0.8846	37029.42	-0.10000	-0.76923
0.9230	42698.29	-0.10000	-0.84615
0.9615	48711.63	-0.10000	-0.92308
1.0000	54986.90	-0.10000	-1

These coefficients were then exported and taken into Curve Fitter to perform the fitting with Flux Exponent n and Regression Rate Coefficient a . The resulting proportionalities with $R^2 = 1$ and $R^2 = 0.998$ respectively were found.

$$k \propto 2.159 * 10^4 * a^2 \quad (3-15)$$

$$q \propto 1 - 2n \quad (3-16)$$

Plugging in the proportionalities found in Eq. (3-15) and Eq. (3-16) into the Belehradek Formula shown in Eq. (3-14) (taking coefficient $p = -0.1$) we get the final form of the control function.

$$\dot{m}_{ox}(t)^* = (2.159 * 10^4 * a^2)(t + 0.1)^{(1-2n)}$$

t – time (3-17)

a – Regression Rate coefficient

n – Flux Exponent

Looking at the new control function, we can already see that an improvement was made compared to the PCF. We have solved the problem of having infinite \dot{m}_{ox} at time $t = 0$ s as well as found a simpler generalized equation with relations to fuel parameters with a higher R^2 than we had with the previous methods. Using Eq. (3-17), we are now able to approximate the TCF as a control function solving the crucial issues of the previous control functions. All that is required to obtain the necessary \dot{m}_{ox} value is to plug in the fuel parameters of choice and plot the function with respect to time. In Figure 21 below we can see the resulted plots of the control function, hereafter called the Belehradek Control Function (BCF).

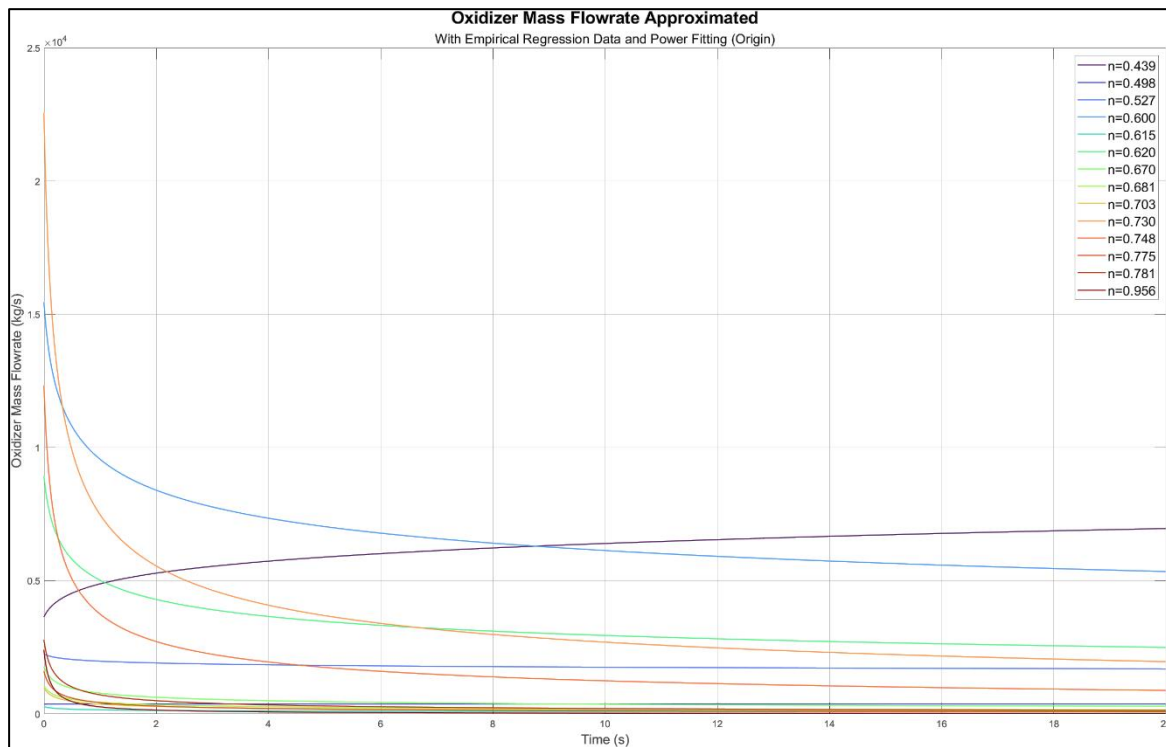


Figure 21: Belehradek Control Function (BCF)

In the following chapter we will finalize the control function by simulating the engine ignition to make sure we are about to take into account that $\dot{m}_{ox} = 0$ when $t = 0$ s. After this is done, we will have a finalized equation which models the ignition process and controls the \dot{m}_{ox} valve

to balance out the **OF** ratio and thereby maximize the Thrust output, negating the effects of fuel regression.

3.2.4 Engine Ignition Modelling

To finalize the control function, we also need to consider the initialization of the engine. We want to consider the fact that the \dot{m}_{ox} value starts from 0 at $t = 0$ s, and then increase that value as some function of time until reaching a point $t = t_{int}$ where the control function and the valve approximation function are equal. The BCF will be used for every point $t > t_{int}$. The Valve Approximation Function (VAF) can be modelled in a few different ways. Flowrate vs valve opening (which can be considered time in our case) of the most common valve types was investigated by P. Arpaia et al [20] in a paper about virtual flow meter-based transducer for gaseous helium monitoring in particle accelerator cryogenics. We can see the characteristics of valve opening vs flow rate for most common valve types mentioned in the paper above in Figure 22 below.

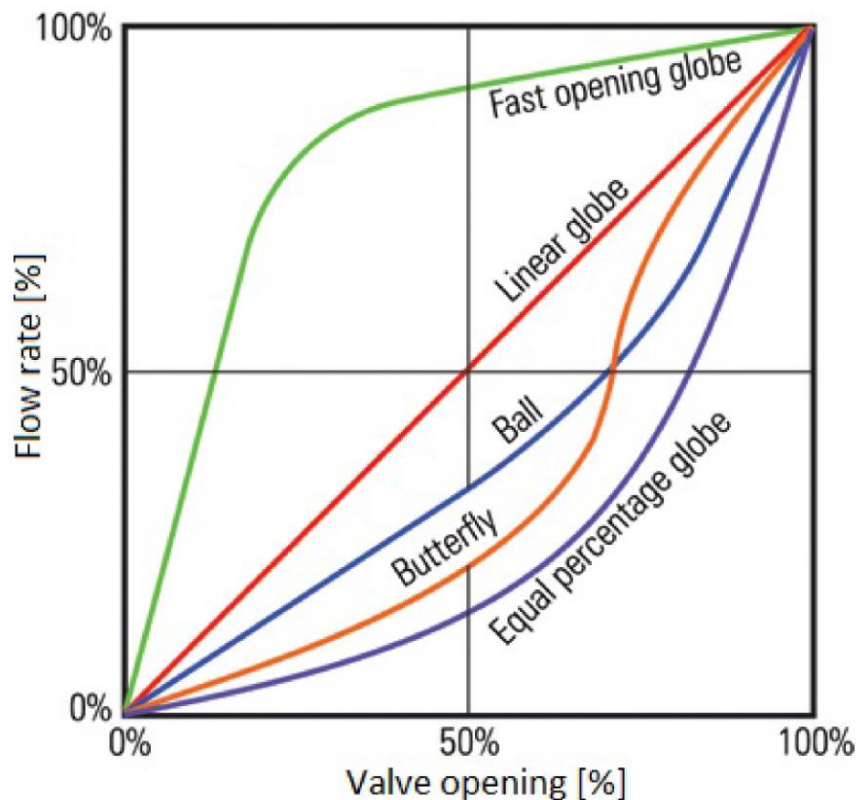


Figure 22: Characteristics of valve opening vs flow rate for most common valve types [20]

Since our oxidizer valve must operate in a fast manner (to ensure responsiveness), a square root model is considered rather than a linear model. The Fast-Opening Globe valve mentioned in Figure 22 comes with unnecessary complexity therefore it is omitted from consideration. Continuing with the square root model we can express the behaviour of the generalized valve in the following way.

$$\dot{m}_{ox}(t)^{v^3} = \sqrt{k_1 t} = k_1 t^{0.5} \quad (3-18)$$

Looking at Eq. (3-18) in comparison with the BCF in Eq. (3-17) we can model the coefficient k_1 in the following way to maintain scaling.

$$k_1 \propto (2.159 * 10^4 * a^2) \quad (3-19)$$

Finalizing the model by combining the proportionality designed in Eq. (3-19) into Eq. (3-18) we get the following final VAF.

$$\dot{m}_{ox}(t)^v = (2.159 * 10^4 * a^2)t^{0.5} \quad (3-20)$$

This approximation when used in combination with the BCF will yield the open-loop controller which was the initial aim of the study.

3.2.5 Prometheus Open Loop Controller

The last step to finalize the open-loop controller is to combine the most optimal results from the previous subchapters with the VAF. Since we have concluded that the CECF and PCF approximations are not optimal in terms of scaling and asymptotic behaviour when $t = 0$ s, we shall form our open-loop controller using the VAF and BCF models. As mentioned in Chapter 3.2.4, the VAF model operates when $t = [0, t_{int}]$ where t_{int} by equating Eq. (3-20) and Eq. (3-17) and solving for time (see equation below for visual aid).

$$(2.159 * 10^4 * a^2)(t + 0.1)^{(1-2n)} - (2.159 * 10^4 * a^2)t^{0.5} = 0 \quad (3-21)$$

³ v – used to indicate valve model

After some simplification we get the following equation, which we use to find t_{int} .

$$(t + 0.1)^{(1-2n)} - t^{0.5} = 0 \quad (3-22)$$

It is visible that time $t = t_{int}$ depends only on the flux exponent of the fuel. After plugging in the exponent necessary and solving the equation numerically we find all the necessary intersection points which we can use to construct the individual function for a particular fuel. The general form of the open-loop controller – hereafter referred to as the Prometheus Open-Loop Controller (POLC) – can be seen in the Eq. (3-23) below.

$$\dot{m}_{ox}(t)_{POLC} = \begin{cases} (2.159 * 10^4 * a^2)t^{0.5}, & t < t_{int} \\ (2.159 * 10^4 * a^2)(t + 0.1)^{(1-2n)}, & t \geq t_{int} \end{cases} \quad (3-23)$$

If we take this equation to MATLAB, and find all intersection points, we can plug in the necessary coefficients for each fuel and plot the results with respect to time to get the \dot{m}_{ox} curves for each type of fuel which can be used to neutralize the **OF** ratio shift, We can see the plots of the POLC function in Figure 23 below.

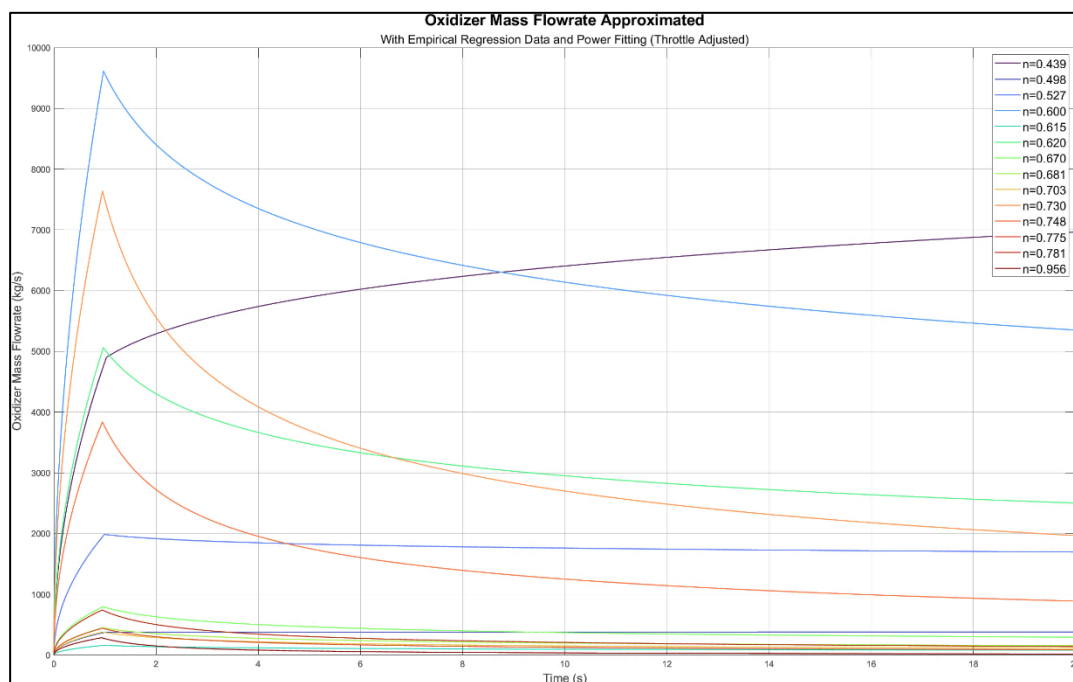


Figure 23: Prometheus Open-Loop Controller (POLC)

These functions can now be used to further analyse the increase in the total impulse with and without the HOLC. These analyses will be conducted in detail with final conclusions and in discussion in Chapter 3.3.

3.2.6 Epimetheus Open Loop Controller

Because of the loss of thrust with the POLC (described in detail in Chapter 4.0), it was decided to also model a different controller that acts on the inverse. Hence the BCF remodelled to operate inversely to the POLC. The IBCF is calculated according to the following equation.

$$\dot{m}_{ox}(t)^* = (2.159 * 10^4 * a^2)(t + 0.1)^{(2n-1)} \quad (3-24)$$

Utilizing Eq. (3-24) we can construct a new model with the following \dot{m}_{ox} relationship with time of the new controller.

$$\dot{m}_{ox}(t)_{EOLC} = \begin{cases} (2.159 * 10^4 * a^2)t^{0.5}, & t < t_{int} \\ (2.159 * 10^4 * a^2)(t + 0.1)^{(2n-1)}, & t \geq t_{int} \end{cases} \quad (3-25)$$

In Eq. (3-25) the t_{int} values need to be recalculated due to the use of the IBCF instead of the BCF. The plots of \dot{m}_{ox} using the EOLC model can be seen in Figure 25 below.

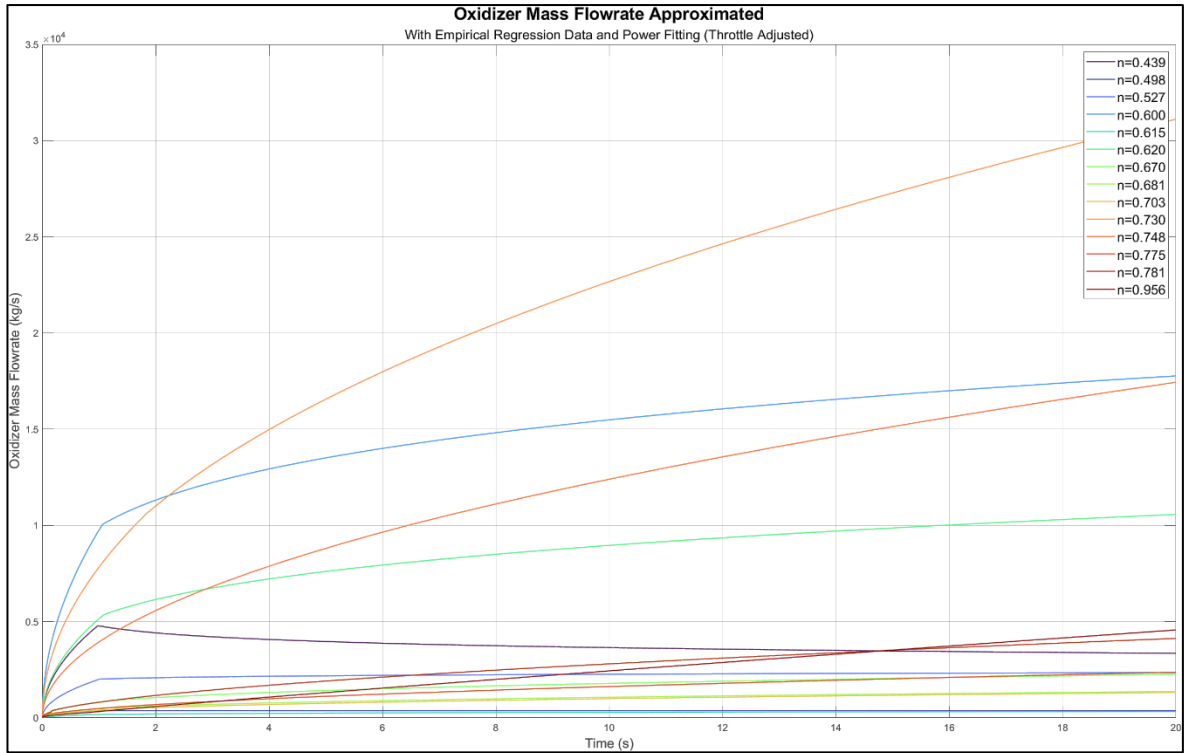


Figure 23: Epimetheus Open-Loop Controller (EOLC)

The thrust calculations and overall effects of the EOLC and POLC on thrust, efficiency, and propellant ratio will be further discussed in the Chapter 3.3 and Chapter 4.0 in greater detail.

3.3 Force Calculations

This chapter will focus on calculating the thrust output of each of these fuels with and without the controller design, to ascertain in the effects of the controller on thrust output, overall engine impulse and propellant ratio shifts.

3.3.1 Calculations without a Controller

To perform the thrust calculations, we must go back to Chapter 2.1. We must use Eq. (2-2) and Eq. (2-7) to get the final form of the thrust equation.

$$F = \dot{m}v_e = \dot{m}_f(OF + 1)v_e \quad (3-26)$$

Given that \dot{m}_f equation with respect to time was defined in Eq. (2-15), we can further transform Eq. (3-26) to become the following.

$$F = \left(2a\pi^{1-n}\rho_f L \dot{m}_{ox}^n \left[a(2n + 1) \left(\frac{\dot{m}_{ox}}{\pi} \right)^n t + R_0^{2n+1} \right]^{\frac{1-2n}{1+2n}} \right) (OF + 1)v_e \quad (3-27)$$

Now we must plug in all the necessary parameters into the equation and view the response with respect to time. Since we are interested in the results without control, we must model the VAF to simulate the engine ignition and after $t = t_{int}$ keep all the \dot{m}_{ox} values constant. This is fully represented in the equation below.

$$\dot{m}_{ox}(t)_{NC^4} = \begin{cases} (2.159 * 10^4 * a^2)t^{0.5}, & t < t_{int} \\ (2.159 * 10^4 * a^2)(t_{int})^{0.5}, & t \geq t_{int} \end{cases} \quad (3-28)$$

Using MATLAB, we can plot the values of the oxidizer for the case with not control given by Eq. (3-28) above. The results of the graphs for all propellant \dot{m}_{ox} values for this case can be seen in Figure 25 below.

⁴ NC – stands for No Control

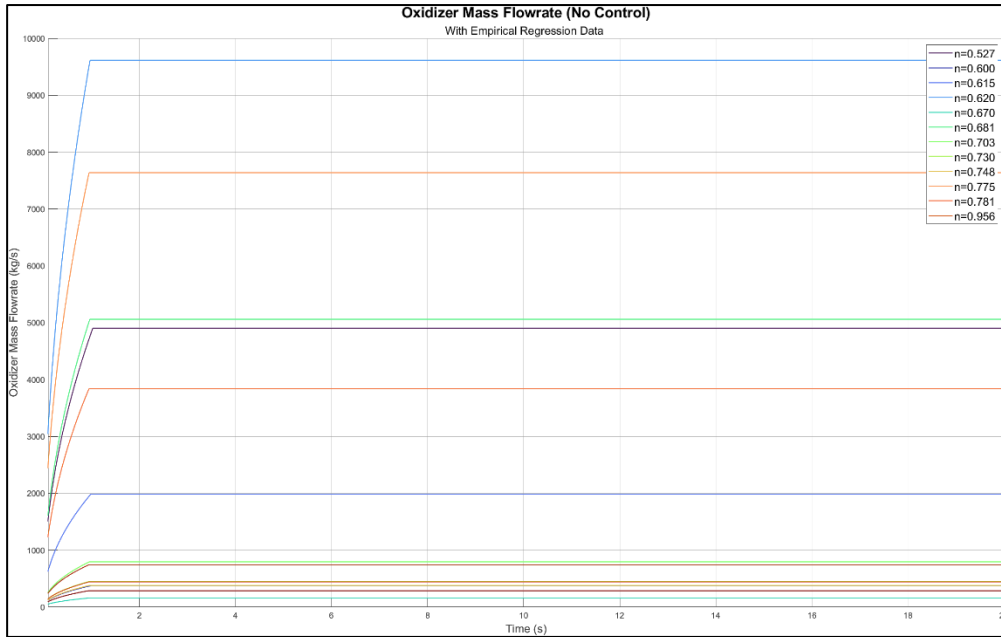


Figure 25: Oxidizer Mass Flowrate (No Control)

Now that the \dot{m}_{ox} has been modelled for the case without control, we use Eq. (3-27) and \dot{m}_{ox} function given by Eq. (3-28) to plot the thrust output for the 14 different fuel types. The plots of the thrust output without control as well as their respective **OF** values can be seen in Figure 26 below. For convenience the propellants with Flux Exponent $n < 0.5$ are plotted on the left side of the figure, and the propellants with $n > 0.5$ are plotted on the right side.

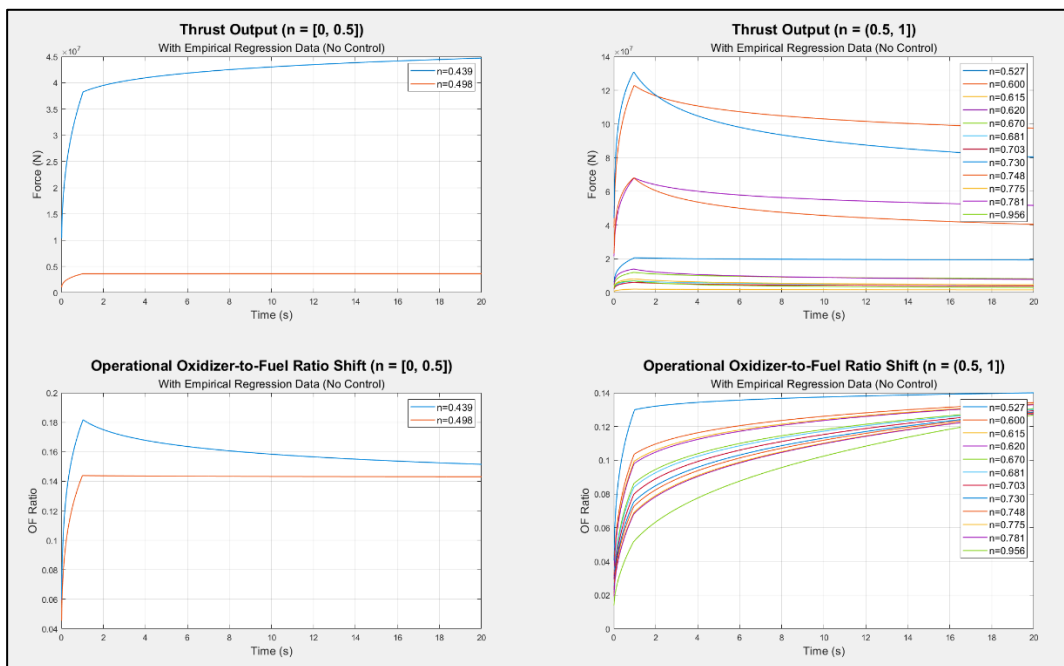


Figure 26: Thrust Calculations (without Control)

Now that we have the thrust values, the same steps can be repeated with the addition of the POLC in the \dot{m}_{ox} value calculations. This will be discussed in Chapter 3.3.2.

The yielded thrust values for each of the propellant types is then numerically integrated to find I_t using the *trapz()* function from the MATLAB library. These values will then be used to compare the efficiency changes with and without the controllers.

3.3.2 Calculations with POLC

To perform the thrust calculations with the POLC, the \dot{m}_{ox} values need to be calculated using Eq. (3-23) and then plugged into Eq. (3-27). After plugging in the necessary parameters for each fuel, the thrust for 14 fuel types is calculated and plotted with respect to time. The POLC thrust calculations can be seen in Figure 27 below.

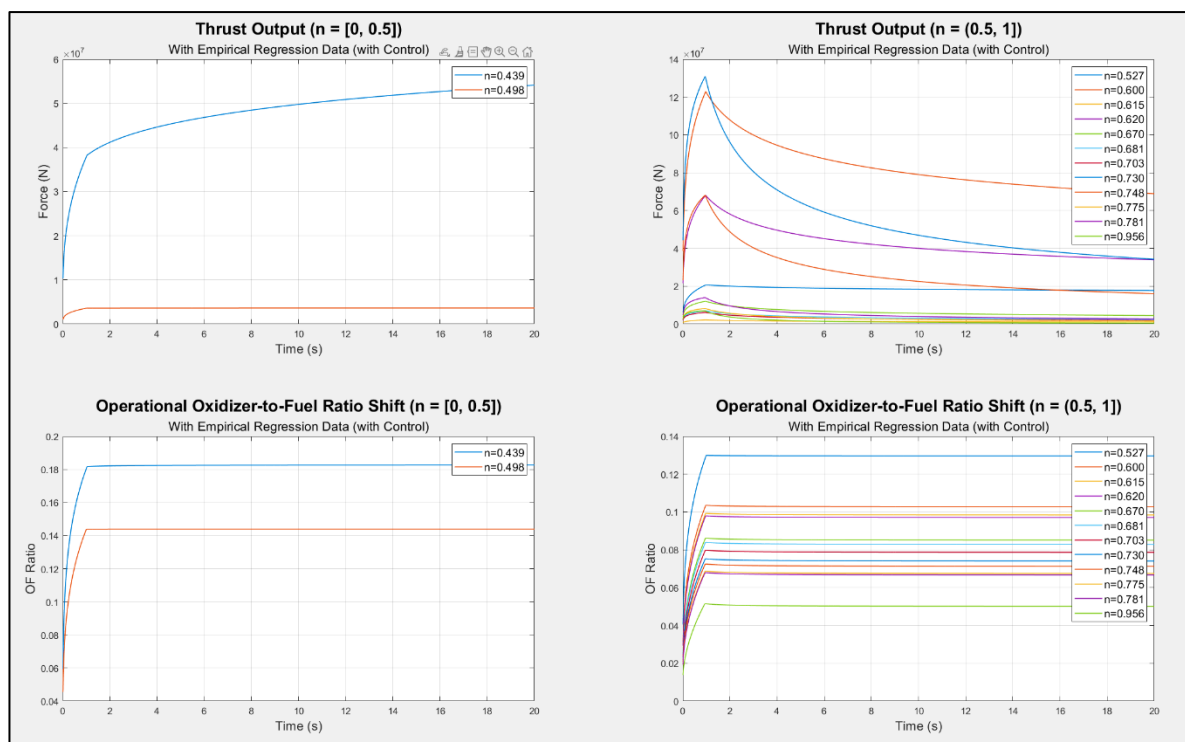


Figure 27: Thrust Calculations (with POLC)

Like the case with no controller, the thrust values for each propellant type are numerically integrated to be later compared in Chapter 4.0 for understanding efficiency change with the addition of the controller.

3.3.3 Calculations with EOLC

For the EOLC, Eq. (3-25) is used to calculate the thrust given by Eq. (3-27). After plugging in all the fuel parameters, the thrust for the 14 different types of fuel was calculated and plotted with respect to time. The plots of the thrust and the respective propellant ratio shifts can be seen in Figure 28 below.

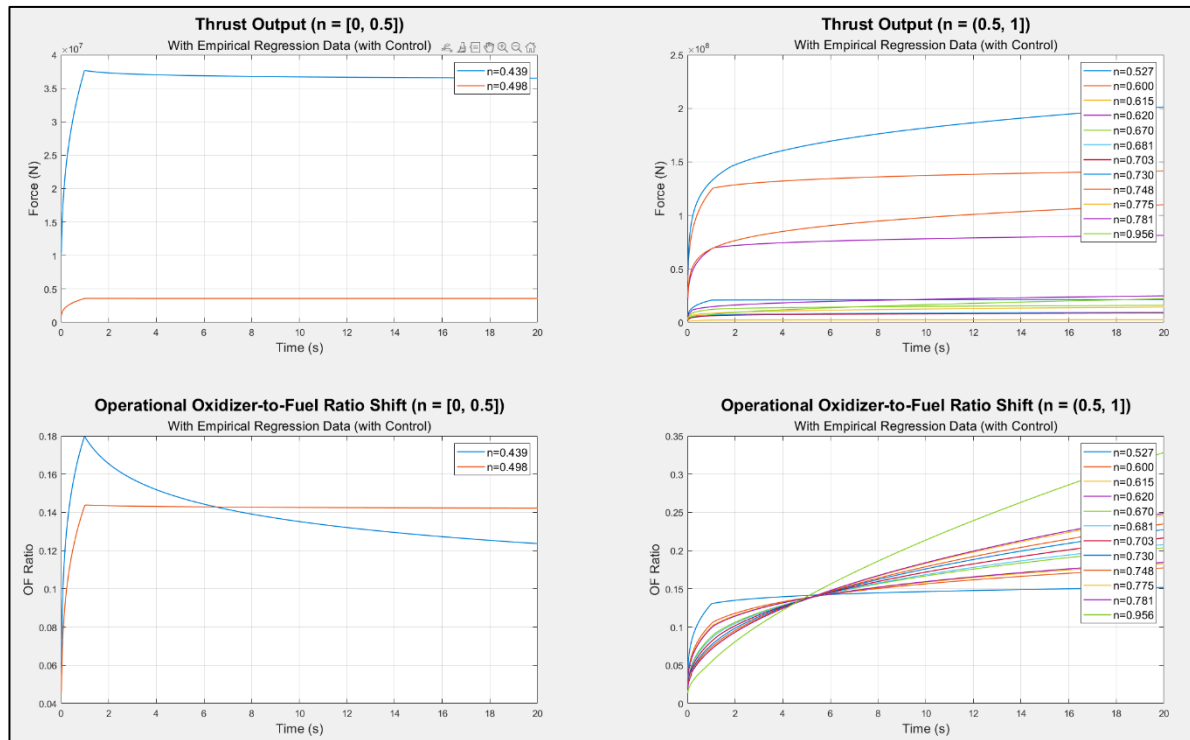


Figure 28: Thrust Calculations (with EOLC)

Just as in the previous two calculations, the thrust values for each propellant are numerically integrated and are to be compared in Chapter 4.0.

4.0 Conclusions and Future Work

4.1 Conclusions

The proposed controllers show interesting results when simulated using the 14 different fuel and HYDRA 3X engine parameters. In this chapter the results of the controllers from Chapter 3.2 will be compared with the operation of the engine without any control in terms of **OF** shift mitigation and I_t variation to have a better understanding of the theoretical performance of these controllers. The results will include calculations for 12 of the original 14 fuels as the fuels with Flux Exponent $n < 0.5$ did not show prominent changes due to their inverse behaviour when it comes to the \dot{m}_f time history.

4.1.1 POLC

The thrust simulations for the POLC controlled engine resulted in the total stability of the **OF** shift which was known theoretically and visible on the thrust plots of the simulations without control. After the modelling of the engine ignition using the VAF ($t = t_{int}$) the increasing trend of the ratio of propellants was halted, and no further shifts were noticeable throughout the 20 seconds of simulated burn time. This is seen in Figure 29-a and Figure 29-b below, where the **OF** plots with respect to time are plotted for the uncontrolled and controlled engines for fuels with Flux Exponent $n > 0.5$.

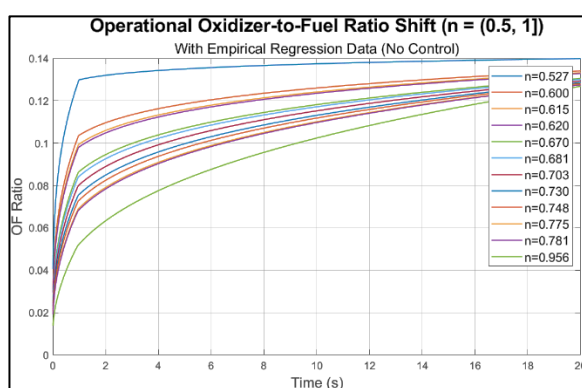


Figure 29-a: OF ratio NC

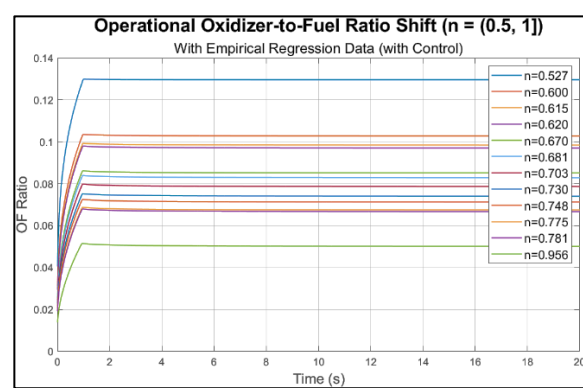


Figure 29-b: OF ratio POLC

These results are expected and show that the controller is indeed successful in eliminating the **OF** shifts. When looking at the I_t values for each fuel calculated in the cases with and without POLC control, undesirable and unfortunate losses in thrust can be noticed. This is due to the

fact that the \dot{m}_{ox} value is being decreased proportionally to the change in \dot{m}_f due to regression. Looking back at Eq. (2-6) we can see how this keeps the **OF** ratio stable, however because of the decrease in both \dot{m}_{ox} and \dot{m}_f , after $t = t_{int}$ the sum of the mass flowrates is less than their sum at any time $t = t - \epsilon$ (where ϵ is a very small increment of time). This results in the total mass flowrate of the system diminishing as a function of time and is observed to be stronger with higher Flux Exponent values of the fuel. In Table 2 below, the I_t values for the controlled and uncontrolled simulations can be seen for 12 of the 14 fuels as well as their respective relative error.

Table 2: POLC vs Uncontrolled Total Impulse

Flux Exponent (n)	I_t Uncontrolled	I_t POLC	Relative Error
0.527	3.92E+08	3.69E+08	0.059
0.6	2.08E+09	1.66E+09	0.203
0.615	3.5E+07	2.7E+07	0.23
0.62	1.12E+09	8.54E+08	0.239
0.67	1.86E+08	1.26E+08	0.32
0.681	1.06E+08	7E+07	0.337
0.703	9.1E+07	5.8E+07	0.369
0.73	1.88E+09	1.12E+09	0.405
0.748	9.58E+08	5.48E+08	0.428
0.775	1.13E+08	6.1E+07	0.46
0.781	1.9E+08	1.01E+08	0.467
0.956	8.1E+07	3.1E+07	0.619

When simulated with the POLC, the engine shows positive relative error for the total impulse of the uncontrolled and controlled cases. This indicates a decrease in efficiency, with a max

decrease by 61.9% when $n = 0.956$. In Figure 30 below we can see the plot of the I_t relative error for the POLC is plotted with respect to the Flux Exponent parameter of the fuel

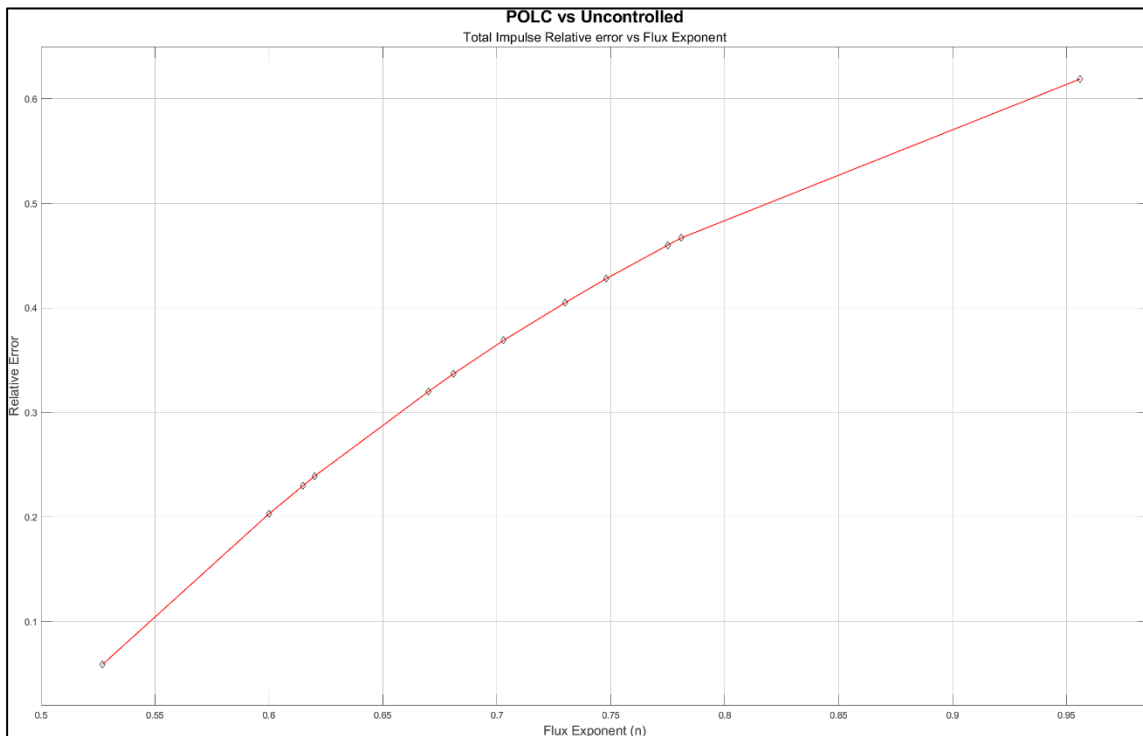


Figure 30: Total Impulse Relative Error vs Flux Exponent (POLC vs Uncontrolled)

From the results of the analysis done above, the loss of I_t requires a different controller to get the desired increase in thrust. For this reason, a modified controller was designed in Chapter 3.2.5, the result analysis of which will be discussed next.

4.1.2 EOLC

The EOLC controlled HYDRA 3X performed incredibly well with regards to thrust increase, though not without its own setbacks. Being remodelled to control the \dot{m}_{ox} in and inversely proportional manner to the \dot{m}_f decrease helped achieve higher thrust values, however, this controller was not able to overcome the OF shifts caused by the fuel regression. Looking at Figure 31-a and Figure 31-b below, we can see the noticeable change in thrust when comparing the EOLC controlled simulation to the uncontrolled simulation, as well as the further destabilization of the OF ratios.

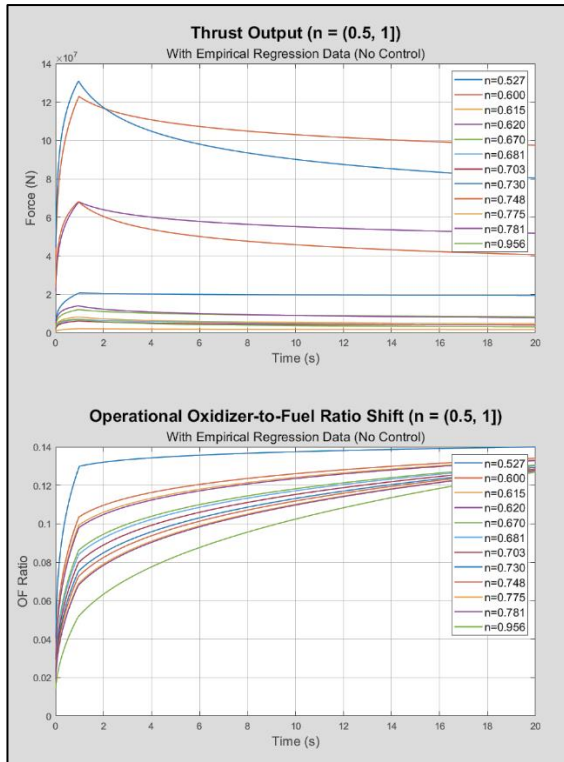


Figure 31-a: Thrust Calculations
Uncontrolled

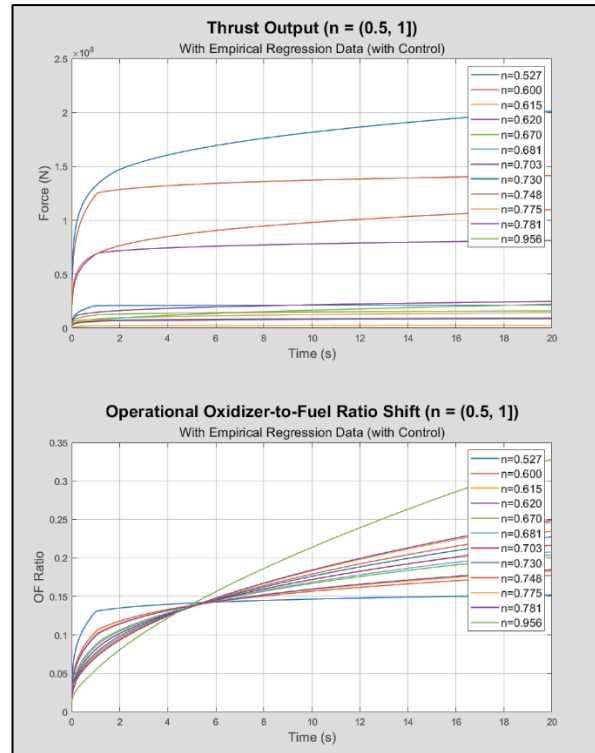


Figure 31-b: Thrust Calculations
EOLC

It can be seen that for each type of fuel tested, the **OF** gets worse after approximately $t = 5.5$ s. This can again be theoretically explained using Eq. (2-6). As for the case with EOLC we are increasing the \dot{m}_{ox} inversely proportional to the decrease in \dot{m}_f , at each point in time we have a worse **OF** shift. Despite that, however, the I_t calculations show the increase in thrust that this controller provides. The data shown in Table 3 below shows the total impulse calculations for the uncontrolled and EOLC controlled simulations as well as their calculated relative error with respect to each other.

Table 3: EOLC vs Uncontrolled Total Impulse

Flux Exponent (n)	I_t Uncontrolled	I_t EOLC	Relative Error
0.527	3.92E+08	4.19E+08	-0.069
0.6	2.08E+09	2.695E+09	-0.293
0.615	3.5E+07	4.8E+07	-0.347
0.62	1.12E+09	1.53E+09	-0.365
0.67	1.86E+08	2.92E+08	-0.571
0.681	1.06E+08	1.7E+08	-0.622
0.703	9.1E+07	1.6E+08	-0.729
0.73	1.88E+09	3.52E+09	-0.873
0.748	9.58E+08	1.89E+09	-0.976
0.775	1.13E+08	2.4E+08	-1.154
0.781	1.9E+08	4.17E+08	-1.194
0.956	8.1E+07	3.2E+08	-2.926

When simulated with the EOLC, the engine shows negative relative error for the total impulse of the uncontrolled and controlled cases. This indicates an increase in efficiency, with the maximum reaching 292.6% with fuels that have a Flux Exponent closer to 1. If we look back at Figure 23, we can see that for the EOLC controlled simulation the \dot{m}_{ox} values are being increased without a limit. On an actual engine the valves for the oxidizer will have a maximum saturation value, past which no more can be added into the engine. Our simulation does not take this into account if it did it is certain that the increase in total impulse will not be this high. To finalize our investigation, we can yet again plot the total impulse relative error with respect to the Flux Exponent values of the fuels to see the relationship the theoretical increase in thrust has with the fuel parameter. We can see the plot mentioned above in Figure 32 below.

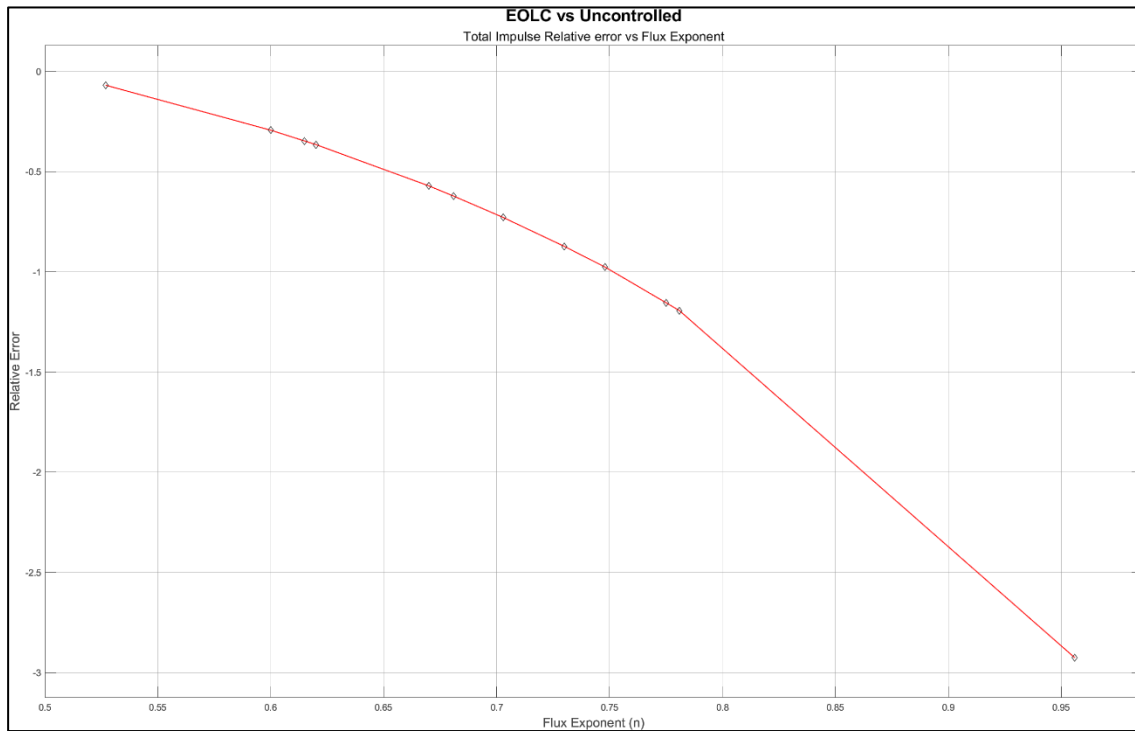


Figure 32: Total Impulse Relative Error vs Flux Exponent (EOLC vs Uncontrolled)

From the analysis above we are able to conclude that the increase in I_t , while large is going to be improbable to replicate in real life at such a scale due to the simulation not taking the valve saturation value into account.

4.1.3 Final Conclusions

From the analysis above we can conclude that each controller was only able to solve one of the two issues this paper focused on. The POLC eliminates the OF ratio shifts completely but exhibits a significant decrease in overall efficiency and thrust when fuels with higher Flux Exponent values are used. The EOLC on the other hand, worsens the OF shifts during operation, but provides a significant theoretical increase in thrust and total impulse of the engine. The actual percentage of the increase in total impulse for the EOLC controlled engine is clear in the scope of this paper as the simulations should be tailored to consider several other factors like valve saturation points, characteristic velocity changes for different fuels, varying stoichiometric OF ratios in the TCF calculations for different fuels, etc.

4.2 Future Work

The future work for this thesis has both experimental and further theoretical components. As mentioned in Chapter 4.1.3, the TCF and thrust simulations need to be further developed to consider oxidizer valve saturations to yield values close to real life. The TCF calculations need to include the proper stoichiometric **OF** ratios for each fuel used to make sure that the data according to which the open loop controllers are modelled is accurate. For the same reason each of the fuels needs to be calculated with different characteristic velocity unique to the fuel type to accurately represent the scale of the thrust curves.

The proposed POLC and EOLC are to be statically tested on a functional HRE with multiple fuels that have known Regression Rate and Flux Exponent coefficients, on a test stand with thrust measuring capability after the improvements mentioned in the paragraph above are completed and satisfactory results are acquired.

The study is to be repeated with and without the controllers to ascertain the deviation from theoretical calculations. This data can then be used to understand the real-life efficiency increase this type of controller has. Since the object of this thesis is an open loop controller, it is not going to be optimal for functional rockets where disturbances can occur at any moment in time. For this reason, a closed loop control needs to be developed using the POLC and/or EOLC as a foundation.

The proposed idea is to try a Model Reference Adaptive Controller (MRAC) design which will have the capability to learn and further improve the gains of the control system during operation. The POLC can be used as a reference model which will provide information on how the system should function, and the disturbance function can be approximated as a relatively large sum of shifted and weighted Gaussian functions. The MRAC version of the Prometheus controller must then again be statically tested on a functional HRE, as well as dynamically tested on a sounding rocket with an HRE on board. The data will then be used to analyze the increase yet again in efficiency as well as the decrease in losses due to disturbances.

References

- [1] Q. Zhao *et al.*, “An Overview of the Applications of Earth Observation Satellite Data: Impacts and Future Trends,” *Remote Sens.*, vol. 14, no. 8, pp. 1–18, 2022, doi: 10.3390/rs14081863.
- [2] NASA, “NASA’s lunar exploration program overview,” *Nasa*, no. September, p. 74, 2020, [Online]. Available: https://www.nasa.gov/sites/default/files/atoms/files/artemis_plan-20200921.pdf
- [3] G. P. Sutton and O. Biblarz, *Rocket Propulsion Elements*, Ninth Edit., vol. 59. Hoboken, New Jersey: Jon Wiley & Sons, Inc., 2016.
- [4] J. D. Hunley, “The history of solid-propellant rocketry: What we do and do not know,” *35th Jt. Propuls. Conf. Exhib.*, 1999, doi: 10.2514/6.1999-2925.
- [5] R. J. Heister, Stephen D.; Anderson, William E.; Pourpoint, Timothée L.; Cassady, *Rocket Propulsion (Cambridge Aerospace Series, Series Number 47)*. 2019. [Online]. Available: www.cambridge.org/9781108422277
- [6] Alliant Techsystems Inc., “ATK Space Propulsion Products Catalog,” vol. 4, no. 08, pp. 1–121, 2008.
- [7] B. P. Mason and C. M. Roland, “Solid propellants,” *Rubber Chem. Technol.*, vol. 92, no. 1, pp. 1–24, 2019, doi: 10.5254/rct.19.80456.
- [8] NASA, “RS – 25,” *National Aeronautics and Space Administration*. NASA, pp. 3–4. [Online]. Available: www.nasa.gov
- [9] L. Alliance and T. Facility, “New SpaceX Raptor engine beats the chamber pressure of Russia’s RD-180 engine, according to Elon Musk,” no. February, pp. 1–3, 2019.
- [10] F. Heeg, L. Kilzer, R. Seitz, and E. Stoll, “Design and test of a student hybrid rocket engine with an external carbon fiber composite structure,” *Aerospace*, vol. 7, no. 5, pp.

- 1–19, 2020, doi: 10.3390/AEROSPACE7050057.
- [11] P. J. Corrigan, “Hybrid rocket propulsion,” *Annu. Rev. Fluid Mech.*, vol. 39, pp. 57–91, 2007.
- [12] J. D. Powell and P. J. Corrigan, “The future of hybrid rocket propulsion,” *Acta Astronaut.*, vol. 73, pp. 456–464, 2013.
- [13] J. T. Buchanan and K. K. Kuo, “Hybrid rocket technology overview,” *Prog. Aerosp. Sci.*, vol. 41, pp. 1–35, 2005.
- [14] Z. J., K. J., and G. Cassella, “Hybrid rocket propulsion,” *J. Propulsion Power*, vol. 23(2), pp. 288–298, 2007.
- [15] M. N. F. Abdullah and M. Z. A. Abidin, “Hybrid rocket engines: A review,” *J. Aerosp. Eng.*, 2011.
- [16] J. C. Poinatte and S. R. Huggins, “Hybrid rocket motor development for reusable launch vehicle applications,” *J. Propuls. Power*, vol. 22(3), pp. 659–665, 2006.
- [17] M. D. Smith and S. P. Wadia, “Hybrid rocket engine technology,” *Encycl. Aerosp. Eng.*, pp. 1–19, 2016.
- [18] H. Tian, X. Meng, H. Zhu, C. Li, L. He, and G. Cai, “Dynamic Numerical Simulation of Hybrid Rocket Motor with HTPB-Based Fuel with 58% Aluminum Additives,” *Aerospace*, vol. 9, no. 11, pp. 1–15, 2022, doi: 10.3390/aerospace9110727.
- [19] G. Zilliac and M. A. Karabeyoglu, “Hybrid rocket fuel regression rate data and modeling,” *Collect. Tech. Pap. - AIAA/ASME/SAE/ASEE 42nd Jt. Propuls. Conf.*, vol. 3, no. May, pp. 1945–1965, 2006, doi: 10.2514/6.2006-4504.
- [20] P. Arpaia *et al.*, “Proof-of-principle demonstration of a virtual flow meter-based transducer for gaseous helium monitoring in particle accelerator cryogenics,” *Rev. Sci. Instrum.*, vol. 86, no. 7, p. 075004, 2015, doi: 10.1063/1.4923466.